



# **N<sub>2</sub>O production and consumption from stable isotopic and concentration data in the Peruvian coastal upwelling system**

Annie Bourbonnais, Robert T. Letscher, Hermann W. Bange, Vincent Echevin, Jennifer Larkum, Joachim Mohn, Naohiro Yoshida, Mark A. Altabet

## **► To cite this version:**

Annie Bourbonnais, Robert T. Letscher, Hermann W. Bange, Vincent Echevin, Jennifer Larkum, et al.. N<sub>2</sub>O production and consumption from stable isotopic and concentration data in the Peruvian coastal upwelling system. *Global Biogeochemical Cycles*, 2017, 31 (4), pp.678 - 698. 10.1002/2016GB005567 . hal-01629665

**HAL Id: hal-01629665**

**<https://hal.science/hal-01629665>**

Submitted on 1 Dec 2021

**HAL** is a multi-disciplinary open access archive for the deposit and dissemination of scientific research documents, whether they are published or not. The documents may come from teaching and research institutions in France or abroad, or from public or private research centers.

L'archive ouverte pluridisciplinaire **HAL**, est destinée au dépôt et à la diffusion de documents scientifiques de niveau recherche, publiés ou non, émanant des établissements d'enseignement et de recherche français ou étrangers, des laboratoires publics ou privés.

Copyright



# Global Biogeochemical Cycles

## RESEARCH ARTICLE

10.1002/2016GB005567

### Key Points:

- High  $N_2O$  concentrations were observed in coastal waters off Peru
- Incomplete denitrifier-denitrification was an important  $N_2O$  production pathway
- $N_2O$  production occurred at high extent of N loss in the shallow ODZ

### Supporting Information:

- Supporting Information S1
- Supporting Information S2

### Correspondence to:

A. Bourbonnais,  
abourbonnais@whoi.edu

### Citation:

Bourbonnais, A., R. T. Letscher, H. W. Bange, V. Échevin, J. Larkum, J. Mohn, N. Yoshida, and M. A. Altabet (2017),  $N_2O$  production and consumption from stable isotopic and concentration data in the Peruvian coastal upwelling system, *Global Biogeochem. Cycles*, 31, 678–698, doi:10.1002/2016GB005567.

Received 3 NOV 2016

Accepted 3 MAR 2017

Accepted article online 7 MAR 2017

Published online 18 APR 2017

## $N_2O$ production and consumption from stable isotopic and concentration data in the Peruvian coastal upwelling system

Annie Bourbonnais<sup>1</sup> , Robert T. Letscher<sup>2</sup> , Hermann W. Bange<sup>3</sup> , Vincent Échevin<sup>4</sup> , Jennifer Larkum<sup>1</sup>, Joachim Mohn<sup>5</sup> , Naohiro Yoshida<sup>6,7</sup> , and Mark A. Altabet<sup>1</sup>

<sup>1</sup>School for Marine Science and Technology, University of Massachusetts Dartmouth, New Bedford, Massachusetts, USA,

<sup>2</sup>Earth System Science, University of California, Irvine, California, USA, <sup>3</sup>GEOMAR, Helmholtz Centre for Ocean Research Kiel, Kiel, Germany, <sup>4</sup>LOCEAN/IRD/IPSL, Laboratoire d'Océanographie et de Climatologie: Expérimentation et Approches Numériques, Paris, France, <sup>5</sup>Empa, Laboratory for Air Pollution and Environmental Technology, Dübendorf, Switzerland,

<sup>6</sup>Department of Chemical Science and Engineering, Tokyo Institute of Technology, Yokohama, Japan, <sup>7</sup>Earth-Life Science Institute, Tokyo Institute of Technology, Tokyo, Japan

**Abstract** The ocean is an important source of nitrous oxide ( $N_2O$ ) to the atmosphere, yet the factors controlling  $N_2O$  production and consumption in oceanic environments are still not understood nor constrained. We measured  $N_2O$  concentrations and isotopomer ratios, as well as  $O_2$ , nutrient and biogenic  $N_2$  concentrations, and the isotopic compositions of nitrate and nitrite at several coastal stations during two cruises off the Peru coast (~5–16°S, 75–81°W) in December 2012 and January 2013.  $N_2O$  concentrations varied from below equilibrium values in the oxygen deficient zone (ODZ) to up to 190 nmol L<sup>-1</sup> in surface waters. We used a 3-D-reaction-advection-diffusion model to evaluate the rates and modes of  $N_2O$  production in oxic waters and rates of  $N_2O$  consumption versus production by denitrification in the ODZ. Intramolecular site preference in  $N_2O$  isotopomer was relatively low in surface waters (generally -3 to 14‰) and together with modeling results, confirmed the dominance of nitrifier-denitrification or incomplete denitrifier-denitrification, corresponding to an efflux of up to 0.6 Tg N yr<sup>-1</sup> off the Peru coast. Other evidence, e.g., the absence of a relationship between  $\Delta N_2O$  and apparent  $O_2$  utilization and significant relationships between nitrate, a substrate during denitrification, and  $N_2O$  isotopes, suggest that  $N_2O$  production by incomplete denitrification or nitrifier-denitrification decoupled from aerobic organic matter remineralization are likely pathways for extreme  $N_2O$  accumulation in newly upwelled surface waters. We observed imbalances between  $N_2O$  production and consumption in the ODZ, with the modeled proportion of  $N_2O$  consumption relative to production generally increasing with biogenic  $N_2$ . However,  $N_2O$  production appeared to occur even where there was high N loss at the shallowest stations.

## 1. Introduction

$N_2O$  is an atmospheric trace gas, mainly produced by microbial processes, that directly and indirectly affects climate. As a tropospheric greenhouse gas, it is ~300 times more potent than  $CO_2$  on a per molecule basis [Forster et al., 2007]. With a long atmospheric residence time (>100 years),  $N_2O$  produced at the planet's surface reaches the stratosphere where it acts as the main source of ozone-depleting nitric-oxide radicals [Nevison and Holland, 1997; Ravishankara et al., 2009]. Microbial processes associated with nitrogen cycling are the dominant natural sources of  $N_2O$ , with those in the open ocean accounting for up to ~35% of global emissions [Forster et al., 2007; Freing et al., 2012; Ciais et al., 2013]. Still, major uncertainties exist in the distribution and magnitude of marine  $N_2O$  production, as important source regions, such as coastal areas, remain poorly characterized [Nevison et al., 1995, 2004].

$N_2O$  is produced in oxic ocean waters as a by-product of nitrifying microbes through decomposition of hydroxylamine, an intermediate during ammonium ( $NH_4^+$ ) oxidation to nitrite ( $NO_2^-$ ) as well as by nitrifier-denitrification, the sequential reduction of  $NO_2^-$  to  $N_2O$  [Frame and Casciotti, 2010] (Figure 1). Accordingly, there are strong positive correlations between apparent oxygen utilization (AOU) and excess  $N_2O$  or  $\Delta N_2O$  (i.e., the difference between  $N_2O$  measured and at equilibrium) and  $NO_3^-$  concentrations [Yoshinari, 1976; Cohen and Gordon, 1979; Nevison et al., 2003].  $N_2O$  production yield from nitrification by

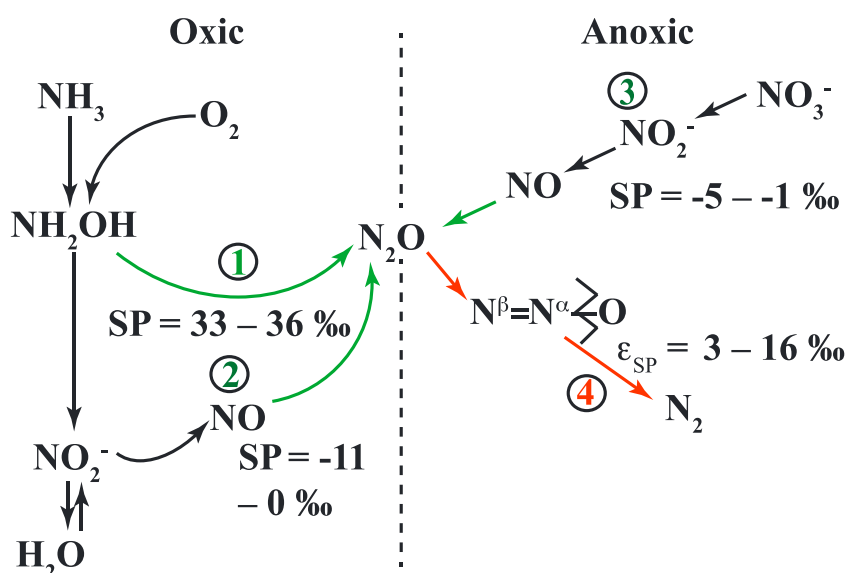


**Figure 1.** Microbial processes involved in marine  $\text{N}_2\text{O}$  production (green) and consumption (red) under oxic ( $[\text{O}_2] > 5 \mu\text{mol L}^{-1}$ ) and anoxic ( $[\text{O}_2] < 5 \mu\text{mol L}^{-1}$ ) conditions and associated SPs. The numbers represent  $\text{N}_2\text{O}$  production by (1) hydroxylamine oxidation, (2) nitrifier-denitrification, and (3) denitrifier-denitrification.  $\text{N}_2\text{O}$  conversion to  $\text{N}_2$  during denitrification is the only process consuming  $\text{N}_2\text{O}$  (4).

either ammonia oxidizing Archaea or Bacteria is generally low, varying from 0 to 2% of  $\text{NO}_3^-$  production [Yoshida *et al.*, 1989; Frame and Casciotti, 2010; Santoro *et al.*, 2010, 2011; Löscher *et al.*, 2012] but has been argued to be enhanced under low- $\text{O}_2$  conditions from both culture and field observations (up to 10% at low  $\text{O}_2$  [Goreau *et al.*, 1980; Ji *et al.*, 2015]). However, other studies have not found such an enhancement [Frame and Casciotti, 2010].

Under anoxic conditions,  $\text{N}_2\text{O}$  may be both produced and consumed during denitrification, the sequential reduction of  $\text{NO}_3^-$ ,  $\text{NO}_2^-$ , NO, to  $\text{N}_2\text{O}$ .  $\text{N}_2\text{O}$  in turn is reduced to nonbioavailable  $\text{N}_2$  (Figure 1). The intermediate NO appears to remain mostly intracellular while  $\text{NO}_2^-$  and  $\text{N}_2\text{O}$  are able to exchange with external pools in the water column. Consequently, in the secondary  $\text{NO}_2^-$  maximum in oxygen deficient zone (ODZ),  $\text{N}_2\text{O}$  is generally near or below atmospheric equilibrium concentrations as a consequence of net removal [Bange *et al.*, 2001; Yamagishi *et al.*, 2007; Babbin *et al.*, 2015; Kock *et al.*, 2016]. Note that the biochemical pathway from  $\text{NO}_2^-$  to  $\text{N}_2\text{O}$  used by denitrifiers in anoxic waters is very similar to the nitrifier-denitrifier pathway in oxic waters.

The highest oceanic concentrations of  $\text{N}_2\text{O}$  and fluxes to the atmosphere have been reported from shallow suboxic waters overlying ODZs of the Indian Ocean, Eastern Tropical North Pacific (ETNP), and Eastern Tropical South Pacific (ETSP) [Naqvi *et al.*, 2000; Arévalo-Martínez *et al.*, 2015; Babbin *et al.*, 2015]. For instance, Arévalo-Martínez *et al.* [2015] observed the highest  $\text{N}_2\text{O}$  accumulations, up to  $1 \mu\text{mol L}^{-1}$ , in surface waters off Peru. These high  $\text{N}_2\text{O}$  accumulations appear to form with changes from anoxic ( $\text{O}_2 = 0 \mu\text{mol L}^{-1}$ ) to suboxic ( $\text{O}_2 < 5 \mu\text{mol L}^{-1}$ ) conditions as denitrifying waters are upwelled. A decoupling between  $\text{N}_2\text{O}$  production and its reduction to  $\text{N}_2$  by denitrification, the latter process being less oxygen tolerant [Dalsgaard *et al.*, 2014], has been considered responsible for elevated  $\text{N}_2\text{O}$  concentrations near the oxycline [Babbin *et al.*, 2015; Ji *et al.*, 2015; Kock *et al.*, 2016].

Stable isotopes are widely used as natural tracers of N-cycle processes in the ocean integrating over their characteristic time and space scales [e.g., Altabet, 2006; Sigman *et al.*, 2005; Bourbonnais *et al.*, 2009, 2015]. Furthermore, natural stable isotope approaches do not suffer from the recognized problems of conventional inhibitor and tracer rate studies including incomplete diffusion of added tracers or inhibitors, alteration of microbial activity due to tracer substrate addition, or other unconstrained bottle effects [Ostrom and Ostrom, 2011].

**Table 1.** Compilation of Isotope Effects and Signatures for N<sub>2</sub>O Production and Consumption (in ‰), i.e., N<sub>2</sub>O Reduction to N<sub>2</sub><sup>a</sup>

<sup>15</sup> ε	<sup>18</sup> ε	SP			Condition	Reference
N <sub>2</sub> O Production by Nitrification						
Nitrifier-Denitrification						
<i>NH<sub>4</sub><sup>+</sup> → N<sub>2</sub>O</i>						
58 ± 4	−8 ± 1	−11 ± 3			<i>Nitrosomonas marina</i>	Frame and Casciotti [2010]
<i>NO<sub>2</sub><sup>−</sup> → N<sub>2</sub>O</i>						
−	−	0 ± 2			<i>Nitrospira multiformis</i>	Sutka et al. [2006]
31–40	−12 – −7	−1 ± 6			<i>Nitrosomonas europaea</i>	Sutka et al. [2003, 2004]
Hydroxylamine Oxidation						
<i>NH<sub>4</sub><sup>+</sup> → N<sub>2</sub>O</i>						
−	3 ± 1	36 ± 2			<i>Nitrosomonas marina</i>	Frame and Casciotti [2010]
47	−	31 ± 4			<i>Nitrosomonas europaea</i>	Sutka et al. [2006]
<i>NH<sub>2</sub>OH → N<sub>2</sub>O</i>						
−2	−	34 ± 1			<i>Nitrosomonas europaea</i>	Sutka et al. [2006]
−2	−	33 ± 1			<i>Nitrospira multiformis</i>	Sutka et al. [2006]
−6	−	36 ± 1			<i>Methylosinus trichosporium</i>	Sutka et al. [2006]
−5–0	−61 – −54	31 ± 6			<i>Methylococcus capsulatus</i>	Sutka et al. [2003, 2004]
7 ± 2 <sup>b</sup>	−	30 ± 1 <sup>b</sup>			<i>Candidatus Nitrosopelagicus brevis</i> CN25	Santoro et al. [2011]
Abiotic Oxidation						
−	−	34–36				Heil et al. [2014]
−	−	30 ± 2				Toyoda et al. [2005]
N <sub>2</sub> O Production by Denitrification						
<i>NO<sub>3</sub><sup>−</sup> → N<sub>2</sub>O</i>						
13	−	−1 ± 2			<i>Pseudomonas chlororaphis</i>	Sutka et al. [2006]
37	−	−1 ± 2			<i>Pseudomonas aureofaciens</i>	Sutka et al. [2006]
10–22	−23 – −4	−5 ± 2			<i>Paracoccus denitrificans</i>	Toyoda et al. [2005]
29 ± 2	−	−			<i>Paracoccus denitrificans</i>	Barford et al. [1999]
N <sub>2</sub> O Consumption by Denitrification						
<sup>15</sup> ε	εα	εβ	<sup>18</sup> ε	εSP		
<i>N<sub>2</sub>O → N<sub>2</sub></i>						
4–8	6–10	2–6	13–19	3–5	soil	Jinuntuya-Nortman [2008]
4	7	2	11	5	<i>Pseudomonas stutzeri</i>	Ostrom et al. [2007]
7	9	2	15	7	<i>Pseudomonas denitrificans</i>	Ostrom et al. [2007]
12 ± 1	20 ± 2	3 ± 0	31 ± 3	16 ± 2	ETNP (advection-diffusion-reaction model)	Yamagishi et al. [2007]
7–10	−	−	13–25	−	soil	Menyailo and Hungate [2006]
6–8	−	−	16–21	−	soil	Menyailo and Hungate [2006]
2	−	−	5	−	landfill soil	Mandernack et al. [2000]
13	−	−	−	−	<i>Pseudomonas denitrificans</i>	Barford et al. [1999]

<sup>a</sup>See Figure 1 for complete reactions.<sup>b</sup>The exact mechanism, isotope effects and SP for N<sub>2</sub>O production by Archaea are still not well constrained.

The N<sub>2</sub>O molecule is uniquely rich in information from stable isotopic composition, containing both bulk (δ<sup>15</sup>N and δ<sup>18</sup>O) and <sup>15</sup>N site specific signatures that are valuable for identifying production and consumption processes. Bulk δ<sup>15</sup>N and δ<sup>18</sup>O are expressed as

$$\delta^{15}\text{N or } \delta^{18}\text{O} = \left( \left( R_{\text{sample}} / R_{\text{reference}} \right) - 1 \right) \times 1000 \quad (1)$$

Units are in parts per thousand or per mil (‰), and *R* is the ratio of <sup>15</sup>N/<sup>14</sup>N or <sup>18</sup>O/<sup>16</sup>O. Reference materials are atmospheric N<sub>2</sub> for N (scale AIR-N<sub>2</sub>) and mean ocean water for O (scale Vienna standard mean ocean water, VSMOW). Site preference (SP) is calculated from the difference in δ<sup>15</sup>N between the central (α) and outer (β) N atoms in the linear, asymmetrical N<sub>2</sub>O molecule (NNO):

$$\text{SP} = \delta^{15}\text{N}^{\alpha} - \delta^{15}\text{N}^{\beta} \quad (2)$$

Nonzero SP arises from the differential biochemical bond making and breaking experienced by each of the two N atoms as a consequence of their different molecular positions (Figure 1). For example, in the consumption of  $\text{N}_2\text{O}$  by denitrification, the bond between the O atom and the  $\alpha$  N atom is broken. It would then be expected that any isotopic fractionation occurring during this process would mostly influence the  $\alpha$  position  $^{15}\text{N}/^{14}\text{N}$  ratio thereby increasing the SP of the residual population of  $\text{N}_2\text{O}$  molecules.

The bulk isotopic composition ( $\delta^{15}\text{N}$  and  $\delta^{18}\text{O}$ ) of  $\text{N}_2\text{O}$  depends in part on the isotopic composition of its substrates (Figure 1). In the case of hydroxylamine oxidation, bulk  $\text{N}_2\text{O}$   $\delta^{15}\text{N}$  and  $\delta^{18}\text{O}$  are functions of the  $\delta^{15}\text{N}$  of the source  $\text{NH}_4^+$  and  $\delta^{18}\text{O}$  of dissolved  $\text{O}_2$ , respectively. For nitrifier-denitrification and denitrification,  $\text{N}_2\text{O}$   $\delta^{15}\text{N}$  and  $\delta^{18}\text{O}$  is dependent on the  $\delta^{15}\text{N}$  and  $\delta^{18}\text{O}$  of source  $\text{NO}_3^-$  and/or  $\text{NO}_2^-$ . A further consideration is that significant O exchange usually occurs between  $\text{NO}_2^-$  and  $\text{H}_2\text{O}$  during  $\text{N}_2\text{O}$  production by nitrifier-denitrification or denitrification [Wrage *et al.*, 2005; Kool *et al.*, 2011; Snider *et al.*, 2012], which would decouple the  $\delta^{18}\text{O}$  values of source and product.

Isotopic fractionation during nitrification and denitrification is the other major influence on the  $\delta^{15}\text{N}$  and  $\delta^{18}\text{O}$  of  $\text{N}_2\text{O}$ . Kinetic isotope fractionation occurs as a consequence of differences in reaction rate for the isotopologues of a molecule (e.g.,  $^{14}\text{N}$ ,  $^{15}\text{N}$  and  $^{16}\text{O}$ ,  $^{18}\text{O}$  for  $\text{N}_2\text{O}$ ). Typically, the molecules containing the lighter isotopes react more quickly leaving the residual substrate enriched in heavier isotopes (e.g.,  $^{15}\text{N}$  and  $^{18}\text{O}$ ). The isotope effect ( $\varepsilon$ ) is defined here by

$$\varepsilon = ((k_1/k_2)-1) \times 1000 \quad (3)$$

where  $k_1$  and  $k_2$  are the reaction rates for the lighter and heavier isotopes, respectively.

N and O isotope effects for ( $^{15}\varepsilon$ ,  $^{18}\varepsilon$ ) during  $\text{N}_2\text{O}$  production and consumption vary substantially in laboratory culture as well as in the environment, likely as a result of sensitivity to growth conditions and reaction rates [Lewicka-Szczepak *et al.*, 2015] and perhaps unconstrained variations in substrate isotopic composition (Table 1). Of course, such variability can complicate the interpretation of field data.

In contrast to bulk isotope values,  $\text{N}_2\text{O}$  SP is independent of the initial isotopic composition of the substrate [Toyoda *et al.*, 2002; Schmidt *et al.*, 2004]. Thus, SP is only process-dependent and can be used as a robust tracer to identify the source of  $\text{N}_2\text{O}$ . For instance, low SP isotopic signatures ( $-11$  to  $0\text{‰}$ ) are associated with  $\text{N}_2\text{O}$  production via  $\text{NO}_2^-$  reduction by nitrifier-denitrification or denitrification. Much higher SP values are indicative of  $\text{N}_2\text{O}$  production by hydroxylamine oxidation ( $30$ – $36\text{‰}$ ) [Sutka *et al.*, 2006; Frame and Casciotti, 2010]. However, SP does increase as a result of isotope fractionation during consumption by denitrification as discussed above [Yamagishi *et al.*, 2005, 2007; Ostrom *et al.*, 2007].

The main goal of this study is to identify the primary sources and sinks for  $\text{N}_2\text{O}$  in coastal waters of the ETSP using a natural stable isotope approach. In particular, we seek to understand the processes leading to near-surface, high  $\text{N}_2\text{O}$  concentrations that could contribute to high fluxes to the atmosphere. We present  $\text{N}_2\text{O}$  concentrations; isotope and isotopomer data for  $\text{N}_2\text{O}$ ,  $\text{NO}_3^-$ , and  $\text{NO}_2^-$ , and other complementary physical and chemical parameters at two high-resolution coastal transects sampled off the coast of Peru in December 2012 (transect A) and January 2013 (transect B, Figure 2). We also used a 3-D-reaction-advection-diffusion regional box model to diagnose physical mixing and biological  $\text{N}_2\text{O}$  fluxes from the field data and evaluate the contribution from different  $\text{N}_2\text{O}$  production processes in oxic and low- $\text{O}_2$  waters and  $\text{N}_2\text{O}$  consumption versus production in the ODZ.

## 2. Materials and Methods

### 2.1. Sample Collection and Hydrographic Data

Samples were collected during two research cruises aboard the R/V *Meteor* on 2 to 23 December 2012 (M91) and 5 to 31 January 2013 (M92) (Figure 2), as part of the German projects SFB 754 (Climate-Biogeochemistry Interactions in the Tropical Ocean) and SOPRAN (Surface Ocean Processes in the Anthropocene). Water samples were collected by using 12 L Niskin bottles ( $\sim 23$  depths per profile) on a conductivity-temperature-depth (CTD) rosette equipped with pressure, conductivity, temperature, and oxygen sensors. Oxygen and nutrient ( $\text{NO}_3^-$ ,  $\text{NO}_2^-$ ,  $\text{NH}_4^+$ , and  $\text{PO}_4^{3-}$ ) concentrations were measured on board as described in Stramma *et al.* [2013].

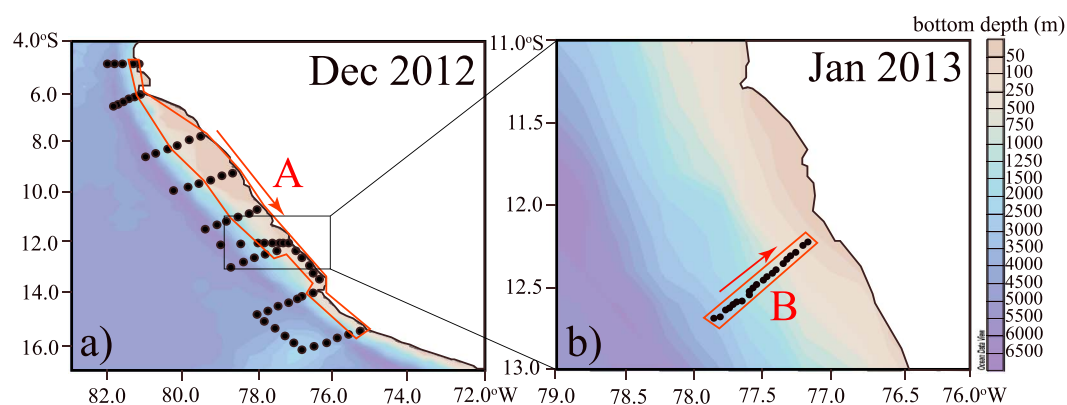


**Figure 2.** Maps showing stations sampled (black dots) during the (a) M91 cruise in December 2012 and (b) M92 cruise in January 2013. The two coastal transects (A and B, red rectangles) used for our analysis are shown.

Samples for dissolved  $\text{N}_2\text{O}$  were collected in a similar fashion as for dissolved  $\text{O}_2/\text{N}_2/\text{Ar}$  samples [see Charoenpong *et al.*, 2014]. Tygon tubing was attached to the Niskin bottle, and a 165 mL serum glass bottle was filled and overflowed with seawater at least 2 times before capping with a butyl stopper and crimp sealed with aluminum seal. This procedure was executed underwater in a plastic container to avoid air bubbles. After collection, 0.2 mL of a saturated  $\text{HgCl}_2$  solution was injected to prevent biological activity.

Samples for  $\text{N}_2/\text{Ar}$  were collected similarly in 60 mL serum glass bottles and preserved with 100  $\mu\text{L}$   $\text{HgCl}_2$  [Charoenpong *et al.*, 2014]. Duplicate  $\text{N}_2/\text{Ar}$  samples were collected at every other depth.

Samples for N and O isotopic composition of  $\text{NO}_3^-$  were collected in 125 mL plastic bottles and acidified for preservation (1 mL of 2.5 mM sulfamic acid in 25% HCl), which also served to remove  $\text{NO}_2^-$  at the time of sample collection [Granger and Sigman, 2009]. For  $\text{NO}_2^-$  isotopic analysis, samples were collected and preserved with NaOH (2.25 mL of 6 M NaOH in 125 mL, pH = 12.5) to prevent oxygen isotope exchange with water during storage [Casciotti *et al.*, 2007]. Samples were stored at room temperature before analysis.

## 2.2. $\text{N}_2\text{O}$ Concentrations, Isotopes, and Isotopomers

Analyses were made by using a GV IsoPrime Continuous Flow, MultiCollector, Isotope-Ratio Mass Spectrometer (CF-MC-IRMS) coupled to an automated gas extraction similar to what is used for  $\text{O}_2/\text{N}_2/\text{Ar}$  samples [Charoenpong *et al.*, 2014], with some modifications. Our IRMS has the necessary collector configuration for simultaneous determination of masses 30, 31 for the  $\text{NO}^+$  fragment of  $\text{N}_2\text{O}$  (determination of  $\delta^{15}\text{N}^a$ ) and 44, 45, and 46 (determination of  $\delta^{15}\text{N}^{\text{bulk}}$  and  $\delta^{18}\text{O}$ ).

Briefly, seawater is pumped from sample bottles through a gas-extractor that is continuously sparged with He. Dissolved  $\text{N}_2\text{O}$  was completely extracted into the He continuous flow and concentrated and purified in a purge-trap system.  $\text{CO}_2$  is chemically removed, and  $\text{H}_2\text{O}$  vapor is eliminated with both chemical and cryogenic traps.  $\text{N}_2\text{O}$  is cryofocused with two liquid  $\text{N}_2$  traps and passed through a capillary gas chromatography (GC) column prior to IRMS analysis. These latter steps are nearly identical to those used by McIlvin and Casciotti [2010] including GC column backflushing to eliminate interferences in the SP determination. For standardization, aliquots of gas standards are injected upstream of the gas-extractor to “experience” all extraction and purification steps.

We calibrated our measurements and corrected for scrambling between the  $\alpha$  and  $\beta$  positions [Westley *et al.*, 2007] using  $\text{N}_2\text{O}$  standards covering a large range of SP (as well as  $\delta^{15}\text{N}^{\text{bulk}}$  and  $\delta^{18}\text{O}$ ) composition (Table 2) [see Mohn *et al.*, 2014]. These standards were analyzed in duplicate for each run to quantify the scrambling effect and potential offsets, and we iteratively solved for the different calibration parameters as described in Frame and Casciotti [2010] and Mohn *et al.* [2014]. Correction for isobaric interference from  $^{17}\text{O}$  is included in these procedures. We have optimized water and He flows to achieve quantitative extraction and reproducibility of results even at low  $\text{N}_2\text{O}$  concentration (down to  $\sim 5 \text{ nmol L}^{-1}$ ). Instrumental drift was determined from measurements of the  $5^\circ\text{C}$  seawater standard distributed throughout an analytical run.

Standard deviations for triplicate measurements of our  $\text{N}_2\text{O}$  standards were typically below 0.1‰ for  $\delta^{15}\text{N}^{\text{bulk}}$ ,  $\text{N}_2\text{O}$ , 0.1‰ for  $\delta^{18}\text{O}-\text{N}_2\text{O}$ , and 1.0‰ for SP, which are comparable to values reported by Mohn *et al.* [2014].



**Table 2.**  $\text{N}_2\text{O}$ ,  $\text{NO}_3^-$ , and  $\text{NO}_2^-$  Standards Used for Sample Calibration (in ‰)

	$\delta^{15}\text{N}^\alpha$	$\delta^{15}\text{N}^\beta$	$\delta^{18}\text{O}$	$\delta^{15}\text{N}^{\text{bulk}}$	SP
$\text{N}_2\text{O}$					
EMPA CB0897	15.7	−3.21	35.2	6.245	18.91
EMPA CB0971	−82.1	−78	21.6	−80.05	−4.1
EMPA CB0976	5.55	−12.9	32.7	−3.675	18.45
EMPA 5350	1.71	94.4	36	48.055	−92.69
$\text{NO}_3^-$					
	$\delta^{15}\text{N}$			$\delta^{18}\text{O}$	
IAEA N3	4.7			25.6	
USGS 34	−1.8			−27.9	
USGS 35	2.7			57.5	
LABmix <sup>a</sup>	38.9			−	
$\text{NO}_2^-$					
	$\delta^{15}\text{N}$			$\delta^{18}\text{O}$	
MAA1 <sup>a</sup>	−60.6			−	
MAA2 <sup>a</sup>	3.9			−	
Zh1 <sup>a</sup>	−16.4			−	
N23	3.7			11.4	
N7272	−79.6			4.5	
N10219	2.8			88.5	

<sup>a</sup>In house standard.

$\text{N}_2\text{O}$  concentrations in our samples were calculated from relative peak heights between the samples and a seawater standard of known  $\text{N}_2\text{O}$  concentration equilibrated with the atmosphere at 5°C ( $12.5 \text{ nmol L}^{-1}$  at salinity 34 as calculated by using the Weiss and Price's [1980] equation). Equilibrium  $\text{N}_2\text{O}$  concentrations were calculated by using the global mean contemporary atmospheric  $\text{N}_2\text{O}$  dry mole fraction of 325 ppb in December 2012 and January 2013 (<http://agage.mit.edu/data/agage-data>). We observed close agreement between the  $\text{N}_2\text{O}$  concentrations measured with our IRMS and those measured independently by Kock *et al.* [2016] by using gas chromatography and an electron capture detector.

### 2.3. Biogenic $\text{N}_2$

$\text{N}_2/\text{Ar}$  and  $\delta^{15}\text{N}-\text{N}_2$  measurements were made on septum-sealed samples by using an online gas extraction system coupled to a CF-MC-IRMS as described in Charoenpong *et al.* [2014]. Excess  $\text{N}_2$  concentration ( $[\text{N}_2]_{\text{excess}}$ ) in  $\mu\text{mol L}^{-1}$ , the observed  $[\text{N}_2]$  minus the equilibrium  $[\text{N}_2]$  at in situ temperature and salinity, was calculated as in Charoenpong *et al.* [2014] and calibrated daily against seawater standards equilibrated with air at fixed temperature. Standard deviation for the samples was generally better than  $0.7 \mu\text{mol L}^{-1}$  for  $[\text{N}_2]_{\text{excess}}$ . We calculated biogenic  $[\text{N}_2]$  ( $[\text{N}_2]_{\text{biogenic}}$ ), the  $[\text{N}_2]$  produced by denitrification or anammox, by subtracting the  $[\text{N}_2]_{\text{excess}}$  at a background station unaffected by N loss from the observed  $[\text{N}_2]_{\text{excess}}$  at corresponding potential density, as in Bourbonnais *et al.* [2015]. This corrects for nonregional biological N loss as well as physically produced deviations in equilibrium  $\text{N}_2/\text{Ar}$  [Hamme and Emerson, 2002].

### 2.4. N and O Isotopic Composition of $\text{NO}_3^-$ and $\text{NO}_2^-$

The stable isotopic compositions ( $\delta^{15}\text{N}$  and  $\delta^{18}\text{O}$ ) of  $\text{NO}_3^-$  and  $\text{NO}_2^-$  were analyzed by using the “bacteria method” [Sigman *et al.*, 2001; Casciotti *et al.*, 2002] and the “azide method” [McIlvin and Altabet, 2005]. For  $\text{NO}_3^-$  isotopic analysis, samples were neutralized and  $\text{NO}_3^-$  was quantitatively converted to  $\text{N}_2\text{O}$  by cultured denitrifying bacteria that lack the active  $\text{N}_2\text{O}$ -reductase enzyme (*Pseudomonas chlororaphis*, ATCC #13985) [Casciotti *et al.*, 2002]. Blank contribution was generally below 5% of the target sample size. For  $\text{NO}_2^-$  isotopic analysis,  $\text{NO}_2^-$  was converted to nitrous oxide ( $\text{N}_2\text{O}$ ) by using sodium azide in acetic acid. The reagent was modified by increasing the acetic acid concentration to 7.84 M to account for high sample pH.  $\text{N}_2\text{O}$  gas was automatically extracted, purified, and analyzed online by using a purge-trap preparation system coupled to an IsoPrime CF-IRMS. Standard sample size was 20 nmol  $\text{N}_2\text{O}$  for  $\text{NO}_3^-$  isotope analysis and 15 nmol  $\text{N}_2\text{O}$  for  $\text{NO}_2^-$  isotope analysis. N and O isotope ratios are reported in per mil (‰), relative to AIR- $\text{N}_2$  for  $\delta^{15}\text{N}$  and to VSMOW for  $\delta^{18}\text{O}$  as in equation (1).

$\text{NO}_3^-$  and  $\text{NO}_2^-$  isotope data were calibrated by using the reference materials listed in Table 2 [see Casciotti and McIlvin, 2007]. The reproducibility was generally better than 0.2‰ for  $\delta^{15}\text{N}$  and 0.5‰ for  $\delta^{18}\text{O}$  in  $\text{NO}_3^-$  and  $\text{NO}_2^-$ .

### 2.5. Regional Box Model Description

We diagnosed the biological fluxes and ratios of  $\text{N}_2\text{O}$  production and consumption processes from the observational data. We accounted for the fluid flow field and physical mixing of  $\text{N}_2\text{O}$  and its isotopomers within

regional box models spanning the spatiotemporal scales of our cruise collected data (see Figure S1 in the supporting information). The physical mixing was estimated by using physical circulation output from an eddy-resolving ROMS (Regional Ocean Modeling System [Shchepetkin and McWilliams, 2005]) simulation. The ROMS model has been used to represent the regional mesoscale circulation in the Peru region with a model configuration similar to that in Penven *et al.* [2005]: it has a  $1/9^\circ \times 1/9^\circ$  spatial resolution ( $\sim 12$  km) and 32 vertical levels with a refined vertical resolution near the surface. For more details on the model configuration, the reader is referred to Penven *et al.* [2005]. This model has been validated against observations in previous works [e.g., Echevin *et al.*, 2011; Montes *et al.*, 2011; Pietri *et al.*, 2014]. Temperature and potential density simulated from the ROMS and observed during both the M91 and M92 cruises agreed well (Figure S2). In the present study, it was forced by monthly open boundary conditions from the  $1/4^\circ$  GLORYS2V3 reanalysis over the period of 2007–2013 operated by Mercator-Ocean and downloaded on the Copernicus platform (<http://marine.copernicus.eu>). Advanced scatterometer daily wind stress processed by Centre ERS d'Archivage et de Traitement (<http://cersat.ifremer.fr/>), climatological heat and freshwater fluxes from Comprehensive Ocean-Atmosphere Data Set [Da Silva *et al.*, 1994], and a restoring of sea surface temperature to advanced very high resolution radiometer optimum interpolation sea surface temperature daily data following Barnier *et al.* [1995], were used at the ocean-atmosphere model interface.

A 70-box model was constructed to encompass the 56 stations sampled for  $\text{N}_2\text{O}$  and its isotopomers during the M91 cruise in December 2012. The 70-box model has dimensions  $7$  (lat)  $\times 2$  (lon)  $\times 5$  (depth), spanning  $5$ – $16^\circ\text{S}$ , oriented at an angle of  $\sim -45^\circ$  from north, which aligns the boxes with the Peru coastline (Figure S3). The longitudinal line separating the inshore (overlying the shelf) boxes from the offshore boxes follows the 300 m isobath. The top of depth level 1 (see Figure S3) begins below the surface mixed layer at 10 m depth as to ignore sea-air gas exchange of  $\text{N}_2\text{O}$  with the atmosphere.

A 25-box model was constructed to encompass the 13 stations sampled for  $\text{N}_2\text{O}$  and its isotopomers during the M92 cruise in January 2013. The 25-box model has dimensions  $5$  (lon)  $\times 5$  (depth, spanning  $5$ – $900$  m) in the region covering  $12.2$  to  $12.8^\circ\text{S}$  and  $77.0$  to  $77.9^\circ\text{W}$ , oriented at an angle of  $\sim +45^\circ$  from north, which aligns the boxes perpendicular with the Peru coastline (Figure S4).

Observed  $[\text{N}_2\text{O}]$ ,  $\delta^{15}\text{N}^\alpha\text{-N}_2\text{O}$ , and  $\delta^{15}\text{N}^\beta\text{-N}_2\text{O}$  were interpolated onto the box model grid and averaged when multiple observations were included in a given model box. Physical mixing of  $\text{N}_2\text{O}$  and its isotopomers by horizontal advection, vertical advection (upwelling), and vertical diffusion between model boxes were considered by using output from a regional ROMS simulation for the months of December 2012 and January 2013. Three-day averaged output of the  $\mathbf{u}$ ,  $\mathbf{v}$ , and  $\mathbf{w}$  velocities (m/s) as well as the log-transformed vertical diffusivity coefficient ( $k_z$ ;  $\text{m}^2/\text{s}$ ) were time averaged to obtain the monthly averaged circulation properties. The  $1/9^\circ$  resolution ROMS output, which lies on a terrain-following (sigma) vertical grid, was interpolated onto the box model grid and averaged for a given model box. Advective velocities and vertical diffusivity were combined with  $[\text{N}_2\text{O}]$  and its isotopomer gradients to compute the physical mixing of tracers between model boxes as

$$\frac{\partial [\text{N}_2\text{O}]_{\text{phy}}}{\partial t} = \nabla \mathbf{u} \text{N}_2\text{O} + \frac{\partial}{\partial z} w \text{N}_2\text{O} + \frac{\partial}{\partial z} k_z \frac{\partial}{\partial z} \text{N}_2\text{O} \quad (4)$$

$$\frac{\partial (\delta^{15}\text{N}^\alpha \times [\text{N}_2\text{O}])_{\text{phy}}}{\partial t} = \nabla (\mathbf{u} \times \delta^{15}\text{N}^\alpha \times \text{N}_2\text{O}) + \frac{\partial}{\partial z} (w \times \delta^{15}\text{N}^\alpha \times \text{N}_2\text{O}) + \frac{\partial}{\partial z} k_z \frac{\partial}{\partial z} (\delta^{15}\text{N}^\alpha \times \text{N}_2\text{O}) \quad (5)$$

with an equation analogous to equation (5) for mixing of  $\delta^{15}\text{N}^\beta\text{-N}_2\text{O}$ . Horizontal diffusion of tracers was not considered, as the ROMS model is eddy-resolving and does not include an explicit diffusion scheme except near the model domain open boundaries [Penven *et al.*, 2005]. The quantity  $\partial [\text{N}_2\text{O}]_{\text{phy}} / \partial t$  was substituted into equations (6)–(9) below to solve for the biological rates producing or consuming  $\text{N}_2\text{O}$ . Anoxic versus oxic boxes in the model were determined by interpolating cruise observed dissolved  $[\text{O}_2]$  onto the model grid by using a  $5 \mu\text{mol L}^{-1}$   $[\text{O}_2]$  cutoff. Boundary fluxes were computed by using ROMS velocities and vertical diffusivity output for the regions immediately to the north, south, and west of the box model domain as well as above (0–10 m depth) and below (300–350 m depth or bottom).  $\text{N}_2\text{O}$  tracer data for the boundary fluxes were taken from the northernmost, southernmost, or westernmost stations as well as the mixed layer (0–10 m) and at depth ( $>300$  m) where available.



The following equations describing the biological fluxes of  $\text{N}_2\text{O}$  and its isotopomers were used in shallow oxic waters ( $[\text{O}_2] > 5 \mu\text{mol L}^{-1}$ ):

$$\frac{\partial[\text{N}_2\text{O}]_{\text{box}}}{\partial t} = \frac{\partial[\text{N}_2\text{O}]_{\text{ND}}}{\partial t} + \frac{\partial[\text{N}_2\text{O}]_{\text{HO}}}{\partial t} + \frac{\partial[\text{N}_2\text{O}]_{\text{phy}}}{\partial t} \quad (6)$$

$$\left( \text{SP}_{\text{box}} \times \frac{\partial[\text{N}_2\text{O}]_{\text{box}}}{\partial t} \right) = \left( \text{SP}_{\text{ND}} \times \frac{\partial[\text{N}_2\text{O}]_{\text{ND}}}{\partial t} \right) + \left( \text{SP}_{\text{HO}} \times \frac{\partial[\text{N}_2\text{O}]_{\text{HO}}}{\partial t} \right) + \left( \frac{\partial(\text{SP} \times [\text{N}_2\text{O}])_{\text{phy}}}{\partial t} \right) \quad (7)$$

where  $\partial[\text{N}_2\text{O}]_{\text{box}}/\partial t$  is the rate of  $\text{N}_2\text{O}$  concentration change for a given model box (sum of biological + mixing terms);  $\text{SP}_{\text{box}}$  is the observed SP for a given box,  $\partial[\text{N}_2\text{O}]_{\text{ND}}/\partial t$ ,  $\partial[\text{N}_2\text{O}]_{\text{HO}}/\partial t$ ,  $\text{SP}_{\text{ND}}$ , and  $\text{SP}_{\text{HO}}$  are the fluxes and SPs from nitrifier-denitrification and hydroxylamine oxidation; and  $\partial(\text{SP} \times [\text{N}_2\text{O}])_{\text{phy}}/\partial t$  represents the physical mixing flux of  $\text{SP} \times [\text{N}_2\text{O}]$  calculated as  $\partial(\delta^{15}\text{N}^{\alpha} \times \text{N}_2\text{O})/\partial t - \partial(\delta^{15}\text{N}^{\beta} \times \text{N}_2\text{O})/\partial t$  (Table 1 and Figure S1).

The following equations were used for ODZ waters ( $[\text{O}_2] < 5 \mu\text{mol L}^{-1}$ ):

$$\frac{\partial[\text{N}_2\text{O}]_{\text{box}}}{\partial t} = \frac{\partial[\text{N}_2\text{O}]_{\text{PD}}}{\partial t} + \frac{\partial[\text{N}_2\text{O}]_{\text{CD}}}{\partial t} + \frac{\partial[\text{N}_2\text{O}]_{\text{phy}}}{\partial t} \quad (8)$$

$$\left( \text{SP}_{\text{box}} \times \frac{\partial[\text{N}_2\text{O}]_{\text{box}}}{\partial t} \right) = \left( \text{SP}_{\text{PD}} \times \frac{\partial[\text{N}_2\text{O}]_{\text{PD}}}{\partial t} \right) - \left( (\text{SP}_{\text{box}} - \varepsilon_D) \times \frac{\partial[\text{N}_2\text{O}]_{\text{CD}}}{\partial t} \right) + \left( \text{SP}_{\text{phy}} \times \frac{\partial[\text{N}_2\text{O}]_{\text{phy}}}{\partial t} \right) \quad (9)$$

where  $\partial[\text{N}_2\text{O}]_{\text{PD}}/\partial t$  and  $\partial[\text{N}_2\text{O}]_{\text{CD}}/\partial t$  are the fluxes from  $\text{N}_2\text{O}$  production and consumption by denitrification,  $\varepsilon_D$  is the isotope effect for SP during denitrification consumption, and  $\text{SP}_{\text{PD}}$  is the SP for denitrification production (Table 1 and Figure S1).

The box model assumes steady state, such that the sum of all fluxes into/out of (mixing) or within a box (biological) equal zero.

### 3. Results

#### 3.1. Distribution of $\text{O}_2$ , Biogenic $\text{N}_2$ , $\text{NO}_3^-$ and $\text{NO}_2^-$ Concentrations and Isotopes

Indicative of intense coastal upwelling, the mixed layer was always relatively shallow, i.e., ~5 m depth for transect A (Figure 3a), and less than 50 m depth at the deepest stations for transect B (Figure 4a). The oxycline ( $[\text{O}_2] < 5 \mu\text{mol L}^{-1}$ ), marking the upper ODZ boundary, became shallower from north to south along transect A varying from ~200 m at 6°S to ~20 to 50 m south of 10°S (Figures 3a and 4a). Along the outer shelf and slope, primary water masses were Antarctic Intermediate Water (AAIW;  $S \approx 34.5$ ,  $T = 5.5^\circ\text{C}$ ) below 500 m and Equatorial Subsurface Water (ESSW;  $34.7 < S < 34.9$ ,  $8.5^\circ\text{C} < T < 10.5^\circ\text{C}$ ) below the thermocline, with the latter corresponding to the low  $\text{O}_2$  core of the southward flowing Peru-Chile Undercurrent (PUC) [Strub *et al.*, 1998]. Peru Coastal Waters (PCW;  $S \approx 35.0$ ,  $T < 19^\circ\text{C}$ ; referred to as Cold Coastal Waters in Pietri *et al.* [2014]) were found next to the coast and mainly resulted from mixing between colder and slightly fresher upwelled waters from the PUC with Subtropical Surface Water (STSW;  $S > 35$ ,  $20^\circ\text{C} < T < 28^\circ\text{C}$ ) [Strub *et al.*, 1998] (Figure 5).

From north to south along transect A, subsurface waters reached the critically low levels of  $\text{O}_2$  required for the onset of N-loss processes (Figure 3). Biogenic  $\text{N}_2$  correspondingly increased as  $\text{NO}_3^-$  was consumed in the ODZ, with a maximum of  $\sim 20 \mu\text{mol L}^{-1}$  at 35 m depth at station 63 (Figure 3c). Relatively high biogenic  $\text{N}_2$  concentrations were also observed in near-surface shelf waters south of 5°S, consistent with upwelling of ODZ waters impacted by N loss (Figures 3a, 3c and 4a, 4c).

This increase in biogenic  $\text{N}_2$  also corresponded to  $\text{NO}_2^-$  accumulations of up to  $11 \mu\text{mol L}^{-1}$  in the coastal ODZ (50 m depth, station 64, transect A; Figure 3b). However, both  $\text{NO}_2^-$  and  $\text{NO}_3^-$  were almost completely consumed ( $< 0.5 \mu\text{mol L}^{-1}$ ) at the shallowest stations (station 63, transect A and station 9, transect B; Figures 3b and 4b), which evidently had the highest extent of N loss.

Nitrate  $\delta^{15}\text{N}$  and  $\delta^{18}\text{O}$  increased with substrate consumption following isotopic fractionation during assimilatory  $\text{NO}_3^-$  reduction by phytoplankton ( $\varepsilon = 5\text{‰}$  [Altabet, 2001]) and dissimilatory  $\text{NO}_3^-$  reduction in the coastal ODZ ( $\varepsilon = 15$  to  $25\text{‰}$  [Brandes *et al.*, 1998; Voss *et al.*, 2001; Granger *et al.*, 2004, 2008; Bourbonnais

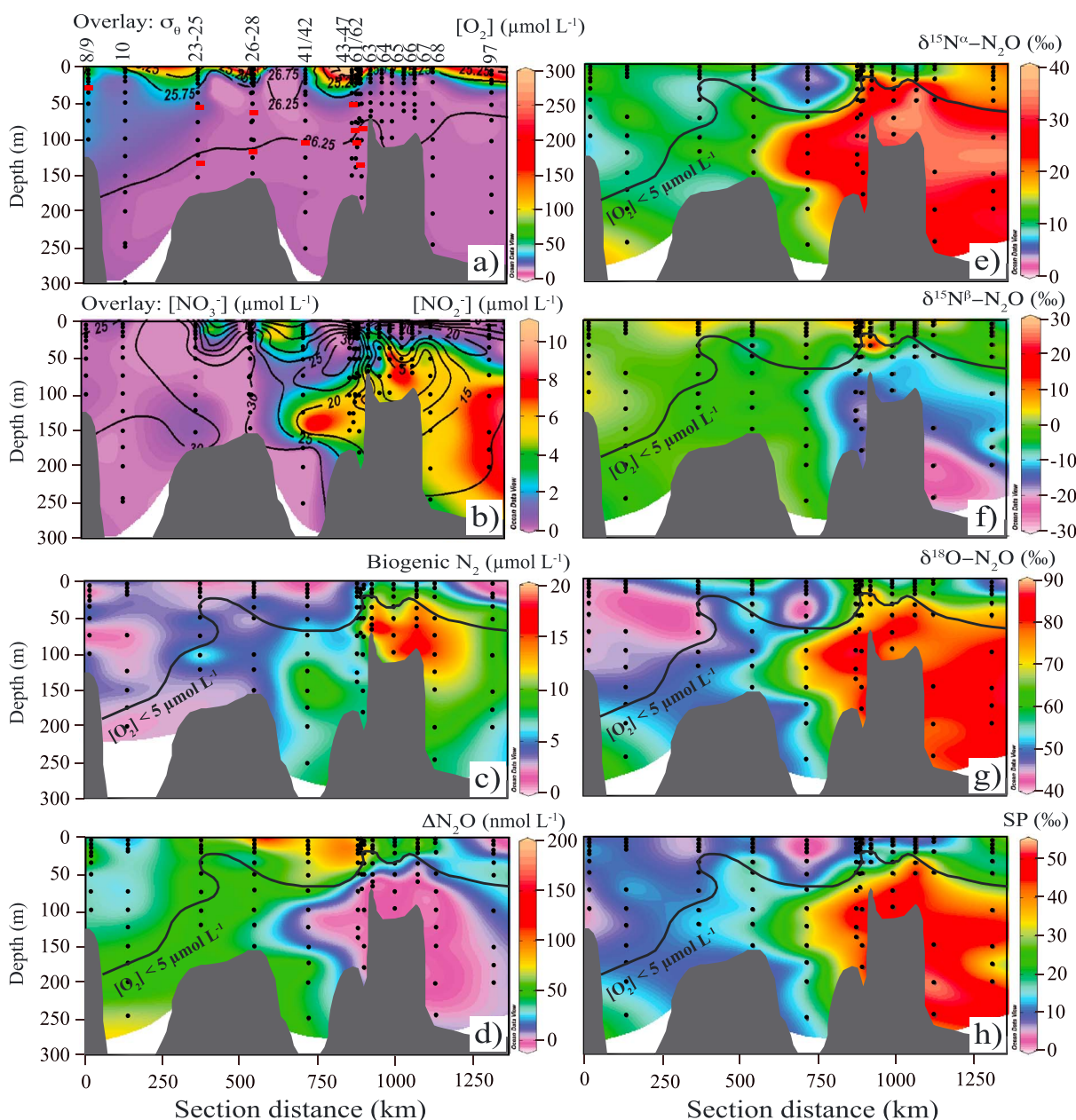


**Figure 3.** Key parameters for transect A along the Peru Coast (see Figure 2). (a)  $[O_2]$  with  $\sigma_\theta$  in overlay, (b)  $[NO_2^-]$  with  $[NO_3^-]$  in overlay, (c) biogenic  $N_2$  (from  $N_2/Ar$  data), (d)  $\Delta N_2O$ , (e)  $\delta^{15}N^{\alpha}-N_2O$ , (f)  $\delta^{15}N^{\beta}-N_2O$ , (g)  $\delta^{18}O-N_2O$ , and (h) SP. In Figure 3a, the depths of the different stations at a given latitude are indicated by red bars. Note that only one station was sampled for  $N_2O$  isotope and isotopomer analysis at a given latitude. CTD numbers are indicated at the top of Figure 3a. Bottom depth was ~300 m at the deepest station 10.

et al., 2015)) (Figures S5a and S5b).  $NO_2^-$   $\delta^{15}N$  also generally increased with substrate consumption, as expected during  $NO_2^-$  reduction ( $\epsilon = 8$  to 22‰ [Bryan et al., 1983; Brunner et al., 2013; Bourbonnais et al., 2015]) (Figures S5c and S5d).

### 3.2. $N_2O$ Concentrations and Isotopomers

During transects A and B, supersaturating  $N_2O$  concentrations as high as  $180 \text{ nmol L}^{-1}$  (station 26, transect A) occurred in oxygenated surface waters at a salinity of ~35 and temperature of ~15°C, characteristic of PCW [Pietri et al., 2014; Kock et al., 2016] (Figure 5) implying high potential fluxes to the atmosphere. In contrast,  $\Delta N_2O$  in the anoxic ODZ decreased from ~60  $\text{nmol L}^{-1}$  (station 10) to below saturating values (down to

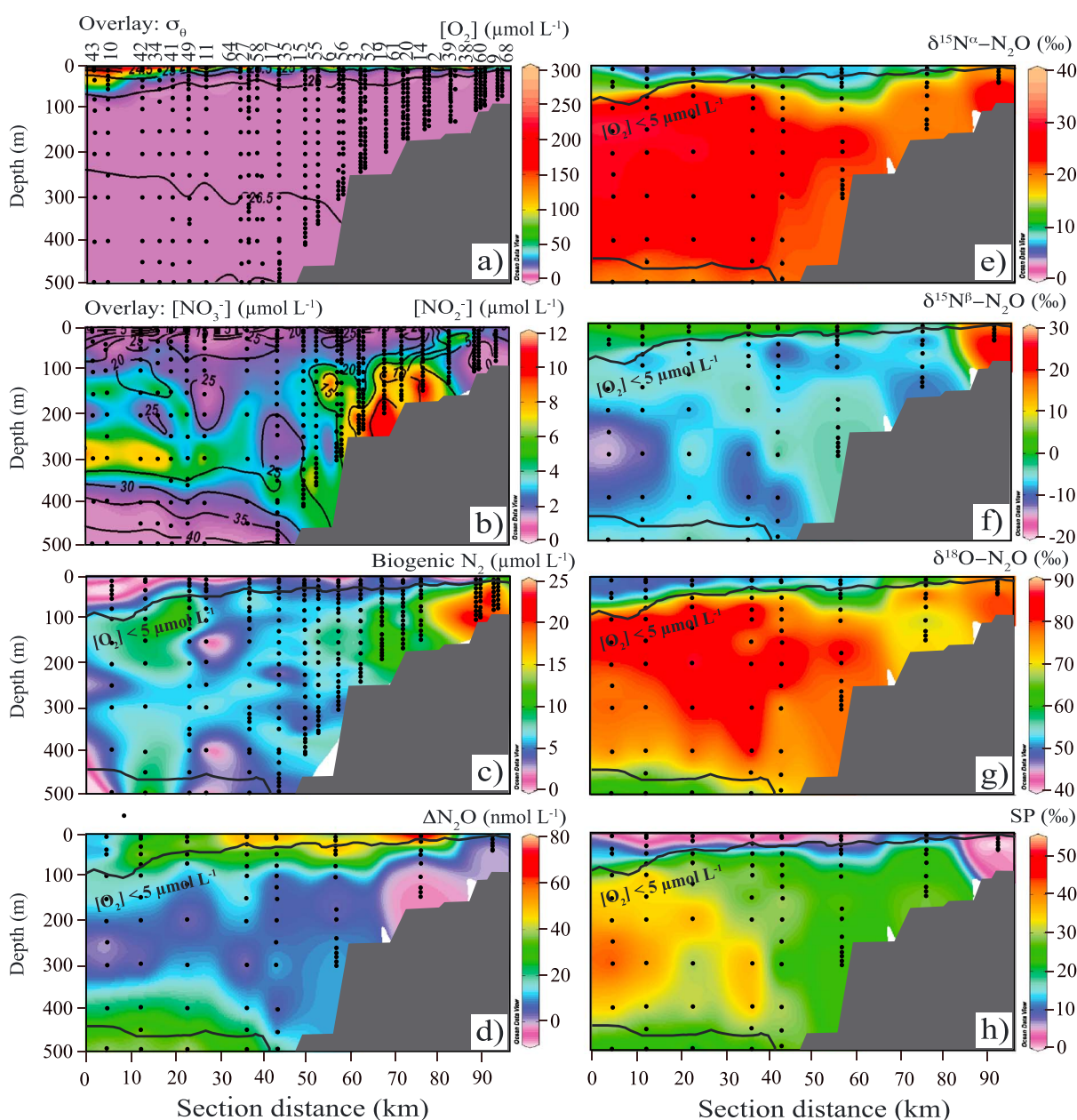


**Figure 4.** Key parameters for transect B normal to the Peru Coast (see Figure 2). (a) [O<sub>2</sub>] with  $\sigma_\theta$  in overlay, (b) NO<sub>2</sub><sup>-</sup> with [NO<sub>3</sub><sup>-</sup>] in overlay, (c) biogenic N<sub>2</sub> (from N<sub>2</sub>/Ar data), (d) ΔN<sub>2</sub>O, (e) δ<sup>15</sup>N<sup>α</sup>-N<sub>2</sub>O, (f) δ<sup>15</sup>N<sup>β</sup>-N<sub>2</sub>O, (g) δ<sup>18</sup>O-N<sub>2</sub>O, and (h) SP. CTD numbers are indicated at the top of Figure 4a. Bottom depth was ~2000 m at the deepest station 43.

−7 nmol L<sup>−1</sup> at station 63) as a consequence of net consumption by denitrification. South of 5°S, the region of low ΔN<sub>2</sub>O expanded vertically along with the ODZ and was correlated with N loss (transect A; Figures 3c and 3d).

Some aspects of our observed coastal distribution of N<sub>2</sub>O have also been found in offshore ODZ studies. North of 5°N in the ETSP a N<sub>2</sub>O maximum of ~60 nmol L<sup>−1</sup> was found in the oxygen minimum but further south a sharp double peak structure formed at the top and bottom of the ODZ with depletion within the core [Cohen and Gordon, 1978; Law and Owens, 1990; Kock et al., 2016]. However, the shapes for the ΔN<sub>2</sub>O in our near-coastal profiles were more variable and not as well defined as compared to offshore with significantly higher ΔN<sub>2</sub>O above the oxycline.

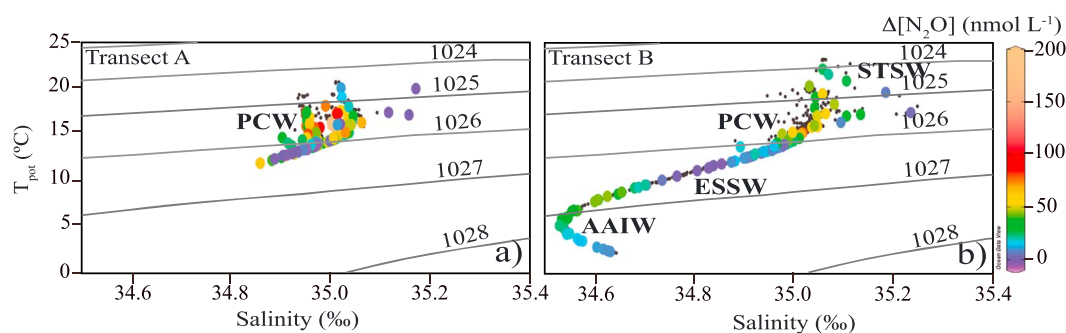


**Figure 5.** Temperature-salinity plots for transects A and B (Figure 2) with color-coded  $\Delta\text{N}_2\text{O}$  (z axis). The grey lines represent  $\sigma_\theta$ . Major water masses are indicated in bold (see section 3.1).

$\text{N}_2\text{O}$  isotopomer composition varied widely along both transects A and B. In oxygenated near-surface waters throughout the study region ( $[\text{O}_2] > 5 \mu\text{mol L}^{-1}$ ),  $\delta^{15}\text{N}^\alpha\text{-N}_2\text{O}$ ,  $\delta^{15}\text{N}^\beta\text{-N}_2\text{O}$ ,  $\delta^{18}\text{O}\text{-N}_2\text{O}$ , and SP varied between 1 to 21‰, −5 to 10‰, 40 to 79‰, and −3 to 26‰, respectively (Figures 3, 4, and 6). The large range in  $\delta^{18}\text{O}\text{-N}_2\text{O}$ , in particular, was directly correlated with biogenic  $\text{N}_2$  concentrations (transect A:  $r^2 = 0.49$ ,  $p\text{-value} < 0.05$ ,  $n = 75$ ; transect B:  $r^2 = 0.76$ ,  $p\text{-value} < 0.05$ ,  $n = 22$ , at  $\text{O}_2 > 5 \mu\text{mol L}^{-1}$ ) and  $\delta^{18}\text{O}\text{-NO}_3^-$  (Figures 7c and 7d). In the ODZ,  $\delta^{15}\text{N}^\alpha\text{-N}_2\text{O}$ ,  $\delta^{18}\text{O}\text{-N}_2\text{O}$ , and SP generally increased to up to 38‰, 93‰, and 56‰, respectively, as N loss increased with vertical expansion of the ODZ south of 5°S along transect A and toward the shelf (transect B). Interestingly,  $\delta^{15}\text{N}^\beta\text{-N}_2\text{O}$  generally remained the same or decreased as  $\delta^{15}\text{N}^\alpha\text{-N}_2\text{O}$  and biogenic  $\text{N}_2$  increased in the coastal and offshore ODZs (Figures 3 and 4).

### 3.3. 3-D Reaction-Advection-Diffusion Box Modeling

The results from our regional box models showed high  $\text{N}_2\text{O}$  production rates of up to  $49 \text{ nmol L}^{-1} \text{ d}^{-1}$  (transect B, Figures 8a and 8e) in oxic waters. These rates were generally higher than those measured by *Ji et al.* [2015] from  $^{15}\text{N}$ -labeled incubations in offshore and coastal oxygenated waters in the ETSP ( $< 1 \text{ nmol L}^{-1} \text{ d}^{-1}$ ).  $\text{N}_2\text{O}$  production mainly occurred through nitrifier-denitrification (or incomplete denitrifier-denitrification as discussed below), which generally represented more than 50% of total  $\text{N}_2\text{O}$  production for transects A and B (Figures 8b and 8f and Tables S1 and S3 in the supporting information).  $\text{N}_2\text{O}$  production rates and the contribution from nitrifier (or incomplete denitrifier)-denitrification were also relatively high where the highest  $\text{N}_2\text{O}$  concentrations were observed (Figure 8).

In comparison, *Frame et al.* [2014] estimated that 64 to 68% of the  $\text{N}_2\text{O}$  production in the isotopic minimum of the upwelling zone off the southern African Coast was from nitrifier-denitrification using a simple model neglecting lateral and vertical advection/diffusion. Using a lower SP of −11‰ (as in *Frame et al.* [2014]) in our model decreased the contribution from nitrifier-denitrification (Tables S1 and S3). In addition, considering only vertical advection/diffusion generally decreased  $\text{N}_2\text{O}$  production rates with no clear effect on the partitioning between nitrifier-denitrification versus hydroxylamine oxidation (Tables S2 and S4). A major difference between both study areas is that in contrast to the upwelling zone off the African Coast, the coastal waters off Peru overlay an ODZ, and therefore, in addition to nitrifier-denitrification,  $\text{N}_2\text{O}$  production is also likely to occur through incomplete denitrifier-denitrification.

$\text{N}_2\text{O}$  production rates in the ODZ derived from our box model were up to  $13.5 \text{ nmol L}^{-1} \text{ d}^{-1}$  when assuming an SP of −0.5‰ for  $\text{N}_2\text{O}$  production by denitrifier-denitrification [*Sutka et al.*, 2006] and an isotope effect of either 5 or 16‰ [*Ostrom et al.*, 2007; *Yamagishi et al.*, 2007] for SP during  $\text{N}_2\text{O}$  consumption by denitrification (Tables S1 and S3). Our  $\text{N}_2\text{O}$  production rates were in the same order of magnitude as those estimated from  $^{15}\text{N}$ -labeled incubations in the ETSP (up to  $\sim 4 \text{ nmol L}^{-1} \text{ d}^{-1}$  [*Ji et al.*, 2015]) and from a 1-D model neglecting lateral advection in the ETNP ODZs (2 to  $35 \text{ nmol L}^{-1} \text{ d}^{-1}$  [*Babbin et al.*, 2015]). Measured  $\text{N}_2\text{O}$  consumption rates from tracer incubations by *Babbin et al.* [2015] in the ETNP ODZ balanced production and also agreed well with our modeled rates (up to  $\sim 40 \text{ nmol L}^{-1} \text{ d}^{-1}$ ; Figures 8c and 8g).

$\text{N}_2\text{O}$  consumption relative to production ranged from 12 to 96% for transect A and 0 to 100% for transect B (Figures 8d and 8h). Assuming a lower isotope effect of 5‰ for SP during  $\text{N}_2\text{O}$  consumption



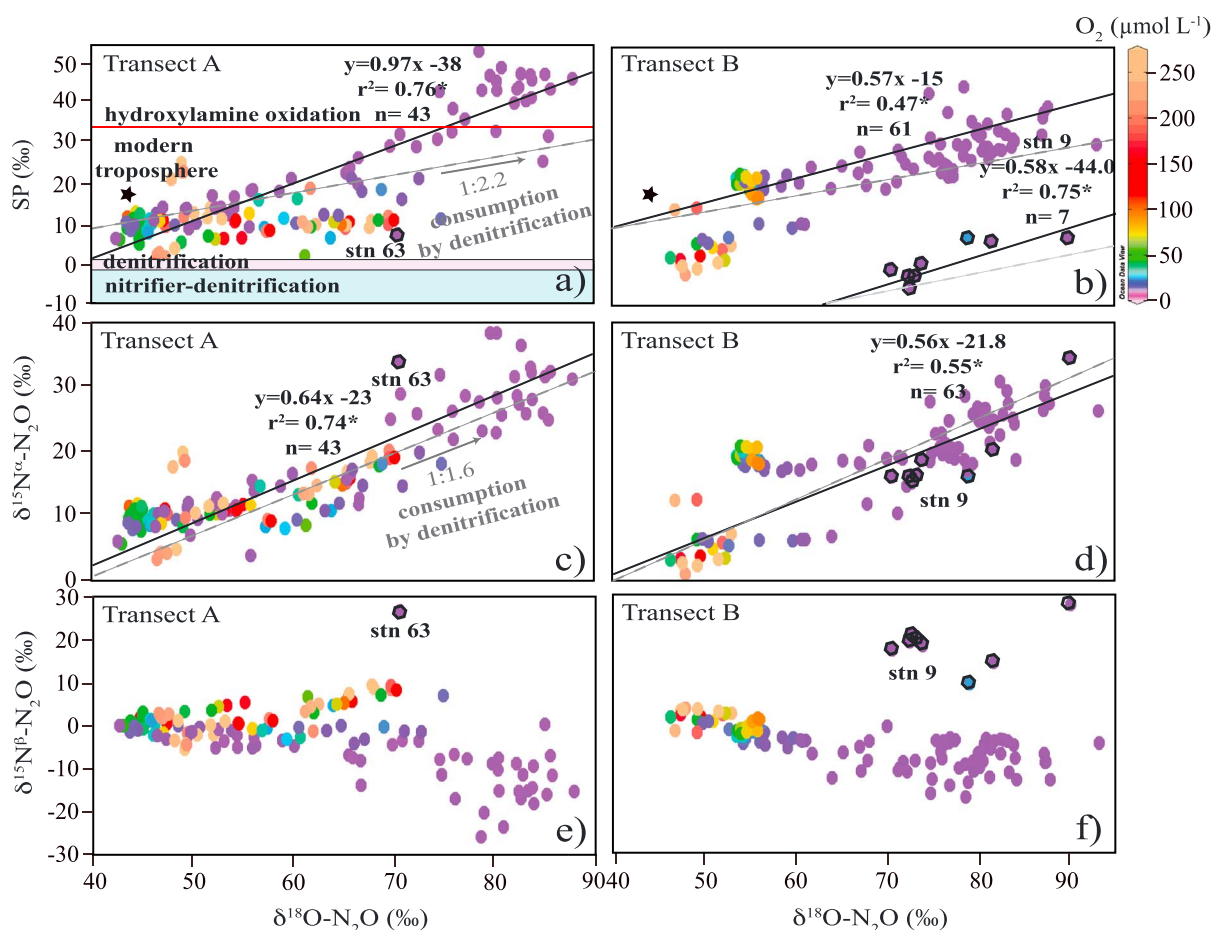


**Figure 6.** (a and b) SP versus  $\delta^{18}\text{O}-\text{N}_2\text{O}$ , (c and d)  $\delta^{15}\text{N}^{\alpha}-\text{N}_2\text{O}$  versus  $\delta^{18}\text{O}-\text{N}_2\text{O}$  and (e and f)  $\delta^{15}\text{N}^{\beta}-\text{N}_2\text{O}$  versus  $\delta^{18}\text{O}-\text{N}_2\text{O}$  for coastal transects A and B with color-coded  $[\text{O}_2]$  (z axis). SP values for  $\text{N}_2\text{O}$  production by hydroxylamine oxidation, nitrifier-denitrification, and denitrification as well as for the modern troposphere (black stars [Yoshida and Toyoda, 2000]) are shown in Figures 6a and 6b. The pale grey dashed lines in Figures 6a–6d are the relationships between SP versus  $\delta^{18}\text{O}-\text{N}_2\text{O}$  and  $\delta^{15}\text{N}^{\alpha}$  versus  $\delta^{18}\text{O}-\text{N}_2\text{O}$  expected during pure  $\text{N}_2\text{O}$  consumption by denitrification. The black lines are the linear regressions for samples with  $[\text{O}_2] < 5 \mu\text{mol L}^{-1}$ . Stars next to  $r^2$  values indicate significant relationships. The hexagons are data points from stations 63 (transect A) and 9 (transect B) showing an increase in  $\delta^{15}\text{N}^{\beta}-\text{N}_2\text{O}$  with  $\delta^{18}\text{O}-\text{N}_2\text{O}$ . Only shelf waters ( $<300$  m depth for transect A and  $<500$  m depth for transect B) were considered.

[Ostrom *et al.*, 2007] increased relative  $\text{N}_2\text{O}$  consumption. The highest relative  $\text{N}_2\text{O}$  consumption in our model also usually occurred at the highest extent of N loss, where  $\text{N}_2\text{O}$  concentrations were below equilibrium, except at the shallowest station 9 (transect B) (Figures 3, 4, and 8).

## 4. Discussion

### 4.1. Extreme $\Delta\text{N}_2\text{O}$ in Upwelling Waters Resulting From Incomplete Denitrification

Throughout most of the ocean, subsurface waters isolated from the atmosphere slowly accumulate  $\text{N}_2\text{O}$  as a by-product of nitrification with progressive organic matter remineralization and  $\text{O}_2$  depletion. The subsurface intermediate waters entering the Peru coastal region in the form of the PUC have already experienced substantial organic matter remineralization since their formation in the Subantarctic and thus enter our study region already low in  $\text{O}_2$  [Strub *et al.*, 1998] and elevated in  $\text{N}_2\text{O}$ . Hence, nitrification during the course of water mass aging both outside as well as within the study region, via either the hydroxylamine oxidation or nitrifier-denitrification [Frame and Casciotti, 2010] pathway is a likely source for positive  $\Delta\text{N}_2\text{O}$  concentrations (up to  $\sim 180 \text{ nmol L}^{-1}$ ). This is particularly so for northern part of transect A which corresponds with the path of the southward flowing PUC.  $\text{N}_2\text{O}$  further accumulates in this portion of transect A where  $\text{N}_2\text{O}$  production is active, but no  $\text{N}_2\text{O}$  consumption occurs, in the absence of denitrification. An exception to this

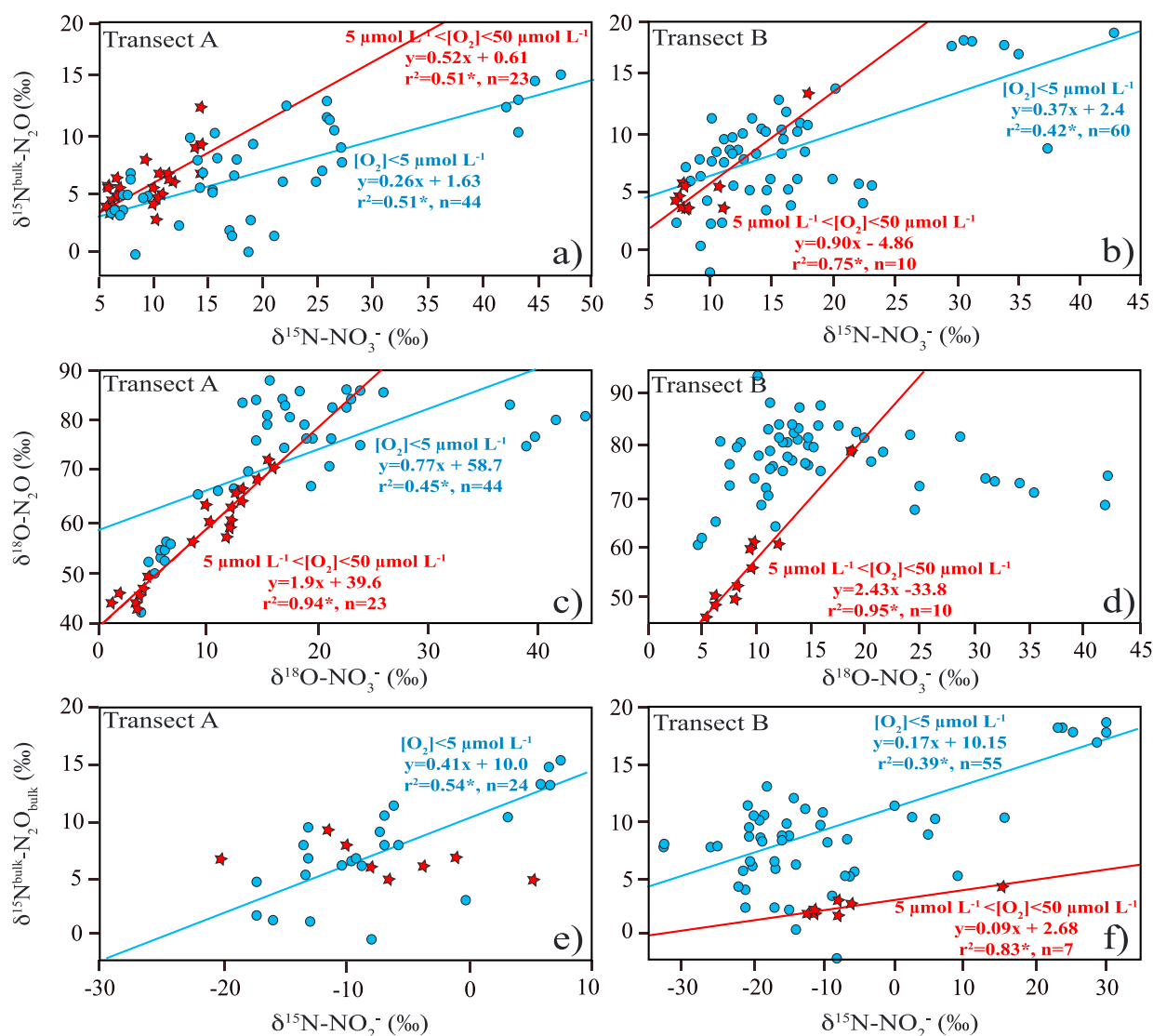


**Figure 7.** (a and b)  $\delta^{15}\text{N}-\text{NO}_3^-$  versus  $\delta^{15}\text{N}^{\text{bulk}}-\text{N}_2\text{O}$ , (c and d)  $\delta^{18}\text{O}-\text{NO}_3^-$  versus  $\delta^{18}\text{O}-\text{N}_2\text{O}$ , and (e and f)  $\delta^{15}\text{N}-\text{NO}_2^-$  versus  $\delta^{15}\text{N}^{\text{bulk}}-\text{N}_2\text{O}$  for transect A and B for  $[\text{O}_2] < 5 \mu\text{mol L}^{-1}$  (blue circles and lines) and  $5 \mu\text{mol L}^{-1} < [\text{O}_2] < 50 \mu\text{mol L}^{-1}$  (red stars and lines). Only coastal waters (<500 m bottom depth) were considered. Stars next to  $r^2$  values indicate significant relationships.

generality are instances of near-surface “hot spots” where incomplete denitrification may lead to some of the highest  $\Delta\text{N}_2\text{O}$  values observed, as upwelled ODZ waters become modestly oxygenated inhibiting  $\text{N}_2\text{O}$  reduction to  $\text{N}_2$  [Arévalo-Martínez et al., 2015; Kock et al., 2016].  $\text{N}_2\text{O}$  may also accumulate disproportionately in our study region where  $\text{O}_2$  is low given the possibility of increasing yield of  $\text{N}_2\text{O}$  production from nitrification under low oxygen concentrations [Goreau et al., 1980; Ji et al., 2015].

As  $\text{N}_2\text{O}$ -SP is only pathway-dependent [e.g., Sutka et al., 2006], it can be used as a robust indicator of source pathway in the absence of consumption by denitrification. Production by nitrifier-denitrification (as well as denitrification) is associated with low SP values of  $-11$  to  $0\text{‰}$ , whereas hydroxylamine oxidation produces higher  $\text{N}_2\text{O}$ -SP values of  $30$ – $36\text{‰}$  [Sutka et al., 2006; Frame and Casciotti, 2010] (Table 1). These laboratory results are mainly for bacterial ammonia oxidizers, whereas archaeal ammonia oxidizers, which are thought to be the dominant nitrifiers in the ocean [Santoro et al., 2011; Löscher et al., 2012], have been shown in culture to produce  $\text{N}_2\text{O}$  with a high SP of  $26$ – $29\text{‰}$ , consistent with a hydroxylamine pathway. However, it was suggested that Archaea could also produce  $\text{N}_2\text{O}$  through  $\text{NO}_2^-$  reduction with lower SP in the environment [Santoro et al., 2011].



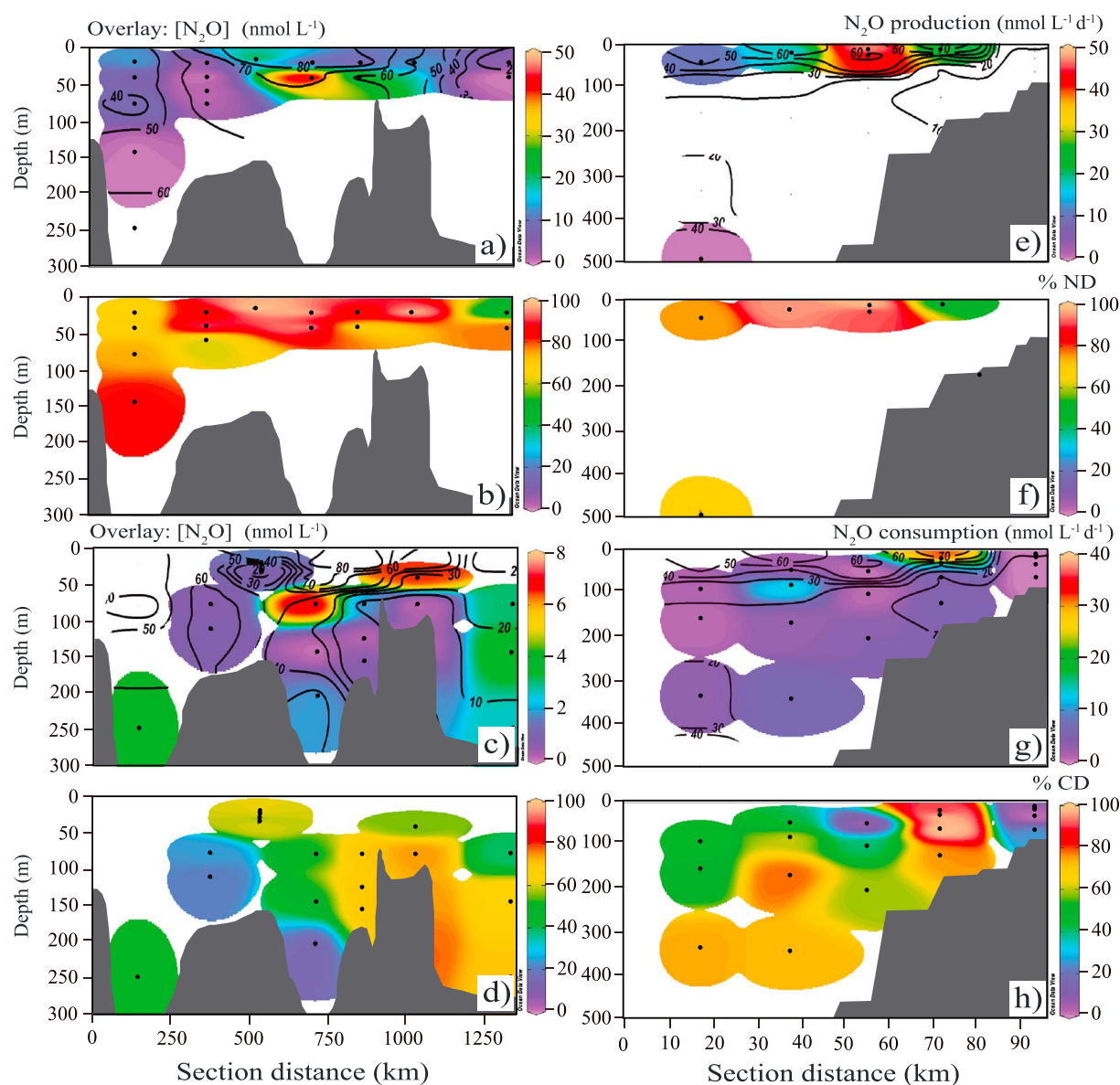


**Figure 8.** Results from the 3-D-reaction-advection-diffusion box models. Profiles of model (a and e) diagnosed rates of  $\text{N}_2\text{O}$  production in oxygenated waters ( $[\text{O}_2] > 5 \mu\text{mol L}^{-1}$ ) with  $\text{N}_2\text{O}$  concentrations in overlay, (b and f) diagnosed %  $\text{N}_2\text{O}$  produced from nitrifier-denitrification (ND) (or incomplete denitrifier-denitrification) relative to total  $\text{N}_2\text{O}$  production assuming a SP of 0‰ for nitrifier-denitrification and 34‰ for hydroxylamine oxidation, (c and g) diagnosed rates of  $\text{N}_2\text{O}$  consumption in the ODZ ( $[\text{O}_2] < 5 \mu\text{mol L}^{-1}$ ) with  $\text{N}_2\text{O}$  concentrations in overlay, and (d and h) diagnosed %  $\text{N}_2\text{O}$  consumption by denitrification (CD) relative to consumption assuming a SP of  $-0.5\text{‰}$  for  $\text{N}_2\text{O}$  production by denitrification and an isotope effect of 16‰ during  $\text{N}_2\text{O}$  consumption along coastal transects A (Figures 8a–8d) and B (Figures 8e–8h). Individual data points represent the average value for each model box (see Figures S3 and S4). See Tables S1 to S3 for sensitivity of results to assuming different SP values and isotope effects.

Throughout the nondenitrifying portions of our study area ( $\text{O}_2 > 5 \mu\text{mol L}^{-1}$ ), relatively low SPs ( $-3$  to  $26\text{‰}$ ) were observed, with most values around  $\sim -3$  to  $14\text{‰}$ , especially for transect A (Figures 3, 4, and 6a, 6b). This and results from our box model (Figures 8b and 8f) suggest that nitrifier (or incomplete denitrifier)-denitrification is the dominant  $\text{N}_2\text{O}$  source.

Prior studies of Peru coastal waters note the occurrence of high  $\Delta\text{N}_2\text{O}$  in oxic ( $[\text{O}_2] > 5 \mu\text{mol L}^{-1}$ ) near-surface waters (up to  $1000 \text{ nmol L}^{-1}$  [see Arévalo-Martínez et al., 2015; Kock et al., 2016]) (Figures 3d and 4d). In both transects A and B, highest  $\Delta\text{N}_2\text{O}$  (up to  $180 \text{ nmol L}^{-1}$ ) is found near surface at a number of stations (Figures 3 and 4). Though representing a minority of our samples, these patches of high  $\text{N}_2\text{O}$  are likely the most

important regional sources of  $\text{N}_2\text{O}$  to the atmosphere and their apparent isolation suggests  $\text{N}_2\text{O}$  production processes unique to them. These high  $\text{N}_2\text{O}$  accumulations likely resulted from a decoupling between  $\text{N}_2\text{O}$  production and consumption by denitrifiers as upwelling ODZ waters are partially re-oxygenated. The largest  $\text{N}_2\text{O}$  accumulations were all observed in the PCW water mass (Figure 5) [Kock *et al.*, 2016] associated with coastal upwelling. Such uncoupling of  $\text{N}_2\text{O}$  production and consumption as a consequence of varying  $\text{O}_2$  has been attributed to incomplete denitrifier (or stop and go)-denitrification [Naqvi *et al.*, 2000; Codispoti *et al.*, 2001]. The threshold  $\text{O}_2$  concentrations for  $\text{N}_2\text{O}$  production and consumption by denitrification are still not well known but appear to be higher for production.  $\text{O}_2$  limits have been reported as high as  $25 \mu\text{mol L}^{-1}$  for  $\text{NO}_3^-$  reduction [Kalvelage *et al.*, 2011] and  $10 \mu\text{mol L}^{-1}$  for  $\text{N}_2\text{O}$  reduction to  $\text{N}_2$  gas [Zamora *et al.*, 2012]. Dalsgaard *et al.* [2014] suggested an even lower  $[\text{O}_2]$  limit for  $\text{N}_2\text{O}$  consumption of  $200 \text{ nmol L}^{-1}$ , which is well below the detection limit of our Seabird  $\text{O}_2$  sensor ( $\sim 3$  to  $5 \mu\text{mol L}^{-1}$ ).

Previously, highest  $\text{N}_2\text{O}$  accumulations have been observed in the coastal upwelling regions off major coastal ODZs, for instance in the Arabian Sea [Naqvi *et al.*, 2010] and in the ETSP off Peru and Chile [Arévalo-Martínez *et al.*, 2015; Farías *et al.*, 2015; Kock *et al.*, 2016], consistent with incomplete denitrifier-denitrification in near-surface waters as a likely important process in these regions. In addition to producing  $\text{O}_2$  transients, coastal upwelling is also associated with high inputs of organic matter and cryptic  $\text{H}_2\text{S}$  cycling [see Canfield *et al.*, 2010], which are substrates during heterotrophic and autotrophic denitrification and can thus also contribute to  $\Delta\text{N}_2\text{O}$  accumulation [e.g., Babbin *et al.*, 2014; Dalsgaard *et al.*, 2014]. Overall, organic matter export and denitrification are particularly enhanced in high productivity shelf regions of ODZ's [e.g., Kalvelage *et al.*, 2013; Babbin *et al.*, 2014].

Given low SP values, the only alternative to incomplete denitrifier-denitrification for these high  $\text{N}_2\text{O}$  accumulations would be nitrifier-denitrification. If we assume that nitrifier-denitrification is coupled to aerobic organic matter remineralization, a relationship between AOU and  $\Delta\text{N}_2\text{O}$  should be observed as reported for offshore waters off Peru [Ryabenko *et al.*, 2012; Kock *et al.*, 2016] and other marine ODZs [Cohen and Gordon, 1978; De Wilde and Helder, 1997; Upstill-Goddard *et al.*, 1999]. Such a relationship was not observed in coastal waters off Peru [Kock *et al.*, 2016; this study]. Instead, the extreme  $\Delta\text{N}_2\text{O}$  observed in shelf surface waters were generally associated with the strongest deviations from the  $\Delta\text{N}_2\text{O}/\text{AOU}$  ratio observed offshore and highest N loss, suggesting that  $\text{N}_2\text{O}$  accumulation likely occurred after re-oxygenation of waters upwelled from the ODZ [Kock *et al.*, 2016].  $^{15}\text{N}$ -labeled incubation experiments by Ji *et al.* [2015] also showed that denitrifier-denitrification was the major  $\text{N}_2\text{O}$  production pathway responsible for at least 50% of total  $\text{N}_2\text{O}$  production just above the ODZ in the ETSP. However, nitrifier-denitrification could be decoupled from aerobic organic matter remineralization if it is fueled by  $\text{NO}_2^-$  produced from  $\text{NO}_3^-$  reduction in the ODZ.

While it is not possible to distinguish between  $\text{N}_2\text{O}$  production by nitrifier-denitrification coupled to aerobic remineralization or denitrifier-denitrification from their isotopomer signatures alone because of their similar low SP (Table 1), our isotopic data do show strong coupling between  $\text{NO}_3^-$  and  $\text{NO}_2^-$  with  $\text{N}_2\text{O}$  in these patches of very high  $\text{N}_2\text{O}$  concentrations. Significant relationships were observed between  $\delta^{15}\text{N}-\text{NO}_3^-$ , and  $\delta^{15}\text{N}-\text{N}_2\text{O}$  at  $\text{O}_2$  concentrations between  $5 \mu\text{mol L}^{-1}$  and  $50 \mu\text{mol L}^{-1}$  at or above the oxycline (Figures 7a and 7b). In particular, highly significant relationships were also observed between  $\delta^{18}\text{O}-\text{NO}_3^-$  and  $\delta^{18}\text{O}-\text{N}_2\text{O}$  for the same  $\text{O}_2$  range (Figures 7c and 7d). As  $\text{NO}_3^-$  is a substrate for  $\text{N}_2\text{O}$  production during denitrification, but not nitrifier-denitrification coupled to aerobic organic matter remineralization, these relationships indicate that high  $\text{N}_2\text{O}$  in near-surface waters likely originated from partly denitrified  $\text{NO}_3^-$  upwelled from the ODZ. In contrast, a relationship between  $\delta^{15}\text{N}-\text{NO}_2^-$ , a substrate during both nitrifier-denitrification and denitrification, and  $\delta^{15}\text{N}-\text{N}_2\text{O}$  was only observed for transect B at  $\text{O}_2$  concentrations between  $5 \mu\text{mol L}^{-1}$  and  $50 \mu\text{mol L}^{-1}$  (Figures 7e and 7f).

No such relationships were observed for  $\text{O}_2 > 50 \mu\text{mol L}^{-1}$ . Phytoplankton  $\text{NO}_3^-$  assimilation and associated fractionation in oxygenated surface waters would likely erase any relationship between  $\text{NO}_3^-$  and  $\text{N}_2\text{O}$  isotopes. However, the high  $\delta^{18}\text{O}-\text{N}_2\text{O}$  (up to 70‰) associated with high  $\text{N}_2\text{O}$  concentrations observed at  $[\text{O}_2] > 50 \mu\text{mol L}^{-1}$  (Figures 3 and 4) suggests that  $\text{N}_2\text{O}$  likely originated from partly denitrified  $\text{NO}_3^-$  enriched in  $^{18}\text{O}$  and was produced at lower  $\text{O}_2$  concentrations near the oxycline before being upwelled to the surface. Overall, our results suggest that incomplete denitrifier-denitrification or nitrifier-denitrification fueled by  $\text{NO}_2^-$  from upwelled ODZ waters are likely pathways for the extreme  $\text{N}_2\text{O}$  accumulation in surface waters off the Peru coast. As  $\text{N}_2\text{O}$  produced in aged source waters is largely consumed in the ODZ (see section 4.2),

these  $\text{N}_2\text{O}$  production mechanisms might represent the major way by which these regions contribute to the ocean's  $\text{N}_2\text{O}$  flux to the atmosphere.

Assuming a total area of  $2.22 \times 10^5 \text{ km}^2$  for the Peruvian upwelling (as in *Arévalo-Martínez et al.* [2015]), a 10 m layer above the ODZ where  $\text{N}_2\text{O}$  production exceed consumption ( $5 \mu\text{mol L}^{-1} > [\text{O}_2] < 25 \mu\text{mol L}^{-1}$ ; from our data and *Babbín et al.* [2015]) and a  $\text{N}_2\text{O}$  production rate of up to  $49 \text{ nmol N}_2\text{O L}^{-1} \text{ d}^{-1}$  in this layer (Figures 8a and 8e), we obtain an efflux of up to  $1.75 \text{ Tg N}_2\text{O yr}^{-1}$  ( $0.6 \text{ Tg N yr}^{-1}$ ). Our estimate is similar to the massive efflux of  $0.2\text{--}0.9 \text{ Tg N yr}^{-1}$  (5 to 22% of previous estimates of global marine  $\text{N}_2\text{O}$  emissions) independently inferred from high-resolution surface measurements and gas exchange parameterizations during the same research expeditions by *Arévalo-Martínez et al.* [2015]. The distinct isotopic signature of marine  $\text{N}_2\text{O}$  produced by incomplete denitrifier-denitrification or nitrifier-denitrification fueled by  $\text{NO}_2^-$  supplied from the ODZ could significantly modify the average atmospheric  $\text{N}_2\text{O}$  isotope and isotopomer composition from river, estuary, and coastal areas over time ( $\delta^{15}\text{N}^{\text{bulk}} = -1.3 \text{ ‰}$ ,  $\delta^{18}\text{O} = 39.1 \text{ ‰}$ , and  $\text{SP} = 23.3 \text{ ‰}$  [*Toyoda et al.*, 2013]), as we generally observed lower SPs and higher  $\delta^{18}\text{O}$  in surface waters (Figures 7a and 7b).

#### 4.2. $\text{N}_2\text{O}$ Consumption and Production by Denitrification in the ODZ

As illustrated in Figures 3 and 4, once  $\text{O}_2$  is  $< 5 \mu\text{mol L}^{-1}$ , N-loss process including denitrification is activated leading to an accumulation of biogenic  $\text{N}_2$  and loss of  $\text{N}_2\text{O}$  as well as an accumulation of  $\text{NO}_2^-$  and isotopic enrichment of both  $\text{NO}_3^-$  and  $\text{NO}_2^-$  (Figure S5). Thus, much if not most of the  $\text{N}_2\text{O}$  accumulated in aging intermediate waters can be consumed by reduction to  $\text{N}_2$  if these waters “terminate” in an ODZ. In this sense, ODZ's could act to reduce the oceanic flux of  $\text{N}_2\text{O}$  to the atmosphere. Assuming an area of  $2.22 \times 10^5 \text{ km}^2$  for the Peruvian upwelling, a maximum layer of 300 m for the ODZ ( $\text{O}_2 < 5 \mu\text{mol L}^{-1}$ ; this study) and a maximum  $\text{N}_2\text{O}$  consumption rate of  $38 \text{ nmol N}_2\text{O L}^{-1} \text{ d}^{-1}$  (Figure 8g), up to  $41 \text{ Tg N}_2\text{O yr}^{-1}$  ( $13 \text{ Tg N yr}^{-1}$ ), could be removed in coastal waters off Peru, which is about 23 times the maximum efflux calculated in this study. In fact, the ODZ layer is generally less than 300 m in coastal areas (see Figures 3 and 4) and  $\text{N}_2\text{O}$  consumption rate generally 1 order of magnitude smaller (see Figures 8c and 8g). This estimate thus represents an absolute upper limit on  $\text{N}_2\text{O}$  loss from the coastal ODZ off Peru.

The isotopomer signals associated with net  $\text{N}_2\text{O}$  consumption are clearly seen in our study region for samples with  $\text{O}_2 < 5 \mu\text{mol L}^{-1}$ .  $\text{N}_2\text{O}$  consumption leads to an increase in SP and  $\delta^{18}\text{O}$  as observed in both transects (Figures 3, 4, and 6). The slopes of the relationships for SP versus  $\delta^{18}\text{O}\text{--}\text{N}_2\text{O}$  were, however, generally greater than the value of 1:2.2 expected for pure  $\text{N}_2\text{O}$  consumption at both transects [*Ostrom et al.*, 2007] (Figures 6a and 6b). Deviation from a slope of 1:2.2 (0.455) for pure  $\text{N}_2\text{O}$  consumption was also observed by *Frame et al.* [2014] for water impacted by denitrification in the South Atlantic and was attributed to mixing and long-range horizontal transport.

As noted above, while  $\delta^{15}\text{N}^{\alpha}$  increased with  $\delta^{18}\text{O}$  in the ODZ,  $\delta^{15}\text{N}^{\beta}$  generally remained the same or decreased (Figures 6e and 6f). It follows that most of the increase in SP with increasing  $\delta^{18}\text{O}$  is due to  $^{15}\text{N}$  enrichment in the  $\alpha$  N atom. A similar trend was also observed at offshore stations in December 2012 (data not shown). From a mechanistic perspective, this is expected as the consumption of  $\text{N}_2\text{O}$  by denitrification involves just the breaking of the bond between the  $\alpha$ -position N and O to produce  $\text{N}_2$  (Figure 1). This observation, though, is only in partial agreement with laboratory observations in which  $\delta^{15}\text{N}^{\alpha}$  and  $\delta^{15}\text{N}^{\beta}$  both increase during  $\text{N}_2\text{O}$  consumption by denitrification but the latter to a lesser degree [*Jinuntuya-Nortman et al.*, 2008; *Ostrom et al.*, 2007; *Yamagishi et al.*, 2007] (Table 1). Such a decrease in  $\delta^{15}\text{N}^{\beta}$  accompanied with increases in  $\delta^{15}\text{N}^{\alpha}$ ,  $\delta^{18}\text{O}$ , and SP was also previously observed in low- $\text{O}_2$  waters ( $< 5 \mu\text{mol L}^{-1}$ ) of the ETNP [*Yamagishi et al.*, 2007] and the Black Sea [*Westley et al.*, 2006] and attributed to shifts from  $\text{N}_2\text{O}$  consumption to net production.  $\text{N}_2\text{O}$  production by denitrification (like the nitrifier-denitrifier pathway) is associated with a low SP of  $\sim 0 \text{ ‰}$  [*Sutka et al.*, 2006] and is thus expected to add almost equally low  $\delta^{15}\text{N}^{\alpha}\text{--}\text{N}_2\text{O}$  and  $\delta^{15}\text{N}^{\beta}\text{--}\text{N}_2\text{O}$ . A shift from  $\text{N}_2\text{O}$  consumption to net production could thus offset the effect of  $\text{N}_2\text{O}$  consumption for  $\delta^{15}\text{N}^{\beta}\text{--}\text{N}_2\text{O}$  and cause it to decrease relative to  $\delta^{15}\text{N}^{\alpha}\text{--}\text{N}_2\text{O}$ .

While net  $\text{N}_2\text{O}$  consumption is observed in the coastal Peru ODZ, denitrifying bacteria must also be producing  $\text{N}_2\text{O}$  (Figure 1) which may exchange with the external pool. In support, *Babbín et al.* [2015] found that  $\text{N}_2\text{O}$  production mostly balanced consumption in the offshore ETNP ODZ based on  $\text{N}_2\text{O}$  reduction rates from tracer incubations and a 1-D model.  $\text{N}_2\text{O}$  concentration profiles at these offshore stations were hence

relatively unchanged over time despite a fast  $\text{N}_2\text{O}$  turnover. In more dynamic coastal ODZ's such as in this study, we observed heterogeneous imbalance between production and consumption from our box model, which is expected as N turnover is generally faster [Hu *et al.*, 2016] and  $\text{N}_2\text{O}$  concentrations in the water column are more spatially and temporally variable [Kock *et al.*, 2016; this study].

Concurrent  $\text{N}_2\text{O}$  production in the ODZ should be evident in coupling of the isotopic signature of  $\text{N}_2\text{O}$  with the signatures of precursor  $\text{NO}_3^-$  and  $\text{NO}_2^-$ .  $\text{NO}_3^-$  and  $\text{NO}_2^-$  increase dramatically in  $\delta^{15}\text{N}$  and  $\delta^{18}\text{O}$  with increasing N loss (Figure S5) following kinetic isotope fractionation. Indeed, significant positive correlations between  $\delta^{15}\text{N}^{\text{bulk-NO}_3^-}$  and  $\delta^{15}\text{N-NO}_3^-$  as well as  $\delta^{15}\text{N-NO}_2^-$  were observed for samples with  $\text{O}_2 < 5 \mu\text{mol L}^{-1}$  for both transects A and B (Figure 7). However, slopes were significantly less than 1 likely indicating other processes simultaneously affecting the substrate and product pools. For instance,  $\text{NO}_2^-$  oxidation to  $\text{NO}_3^-$  is associated with an inverse  $^{15}\text{N}$  kinetic isotope effect of  $-13\text{‰}$  (Casciotti, 2009) and thus raises the  $\delta^{15}\text{N-NO}_3^-$  and lowers the  $\delta^{15}\text{N-NO}_2^-$ . Similarly,  $\text{N}_2\text{O}$  consumption enhances  $\delta^{15}\text{N-N}_2\text{O}$  as discussed earlier. Different degrees of  $\text{NO}_2^-$  re-oxidation and  $\text{N}_2\text{O}$  consumption at non-steady state conditions could thus cause the  $\delta^{15}\text{N-N}_2\text{O}/\delta^{15}\text{N-NO}_3^-$  and  $\delta^{15}\text{N-N}_2\text{O}/\delta^{15}\text{N-NO}_2^-$  slopes to deviate from 1. It is, however, not clear why, for the same sample set,  $\delta^{18}\text{O-N}_2\text{O}$  and  $\delta^{18}\text{O-NO}_3^-$  appeared to be positively correlated only at low  $\delta^{18}\text{O-NO}_3^-$  values. In addition to kinetic isotope effects [see Frame and Casciotti, 2010],  $\delta^{18}\text{O}$  of  $\text{N}_2\text{O}$  is impacted by branching isotope effects during  $\text{NO}_3^-$  and  $\text{NO}_2^-$  reduction to  $\text{N}_2\text{O}$ , that elevate the  $\delta^{18}\text{O}$  of  $\text{N}_2\text{O}$  relative to its  $\delta^{15}\text{N}$  [Casciotti *et al.*, 2007]. The  $\text{NO}_2^-$  oxygen atoms also tend to slowly equilibrate with water on a time scale of weeks to months, depending on in situ temperature and pH, with a  $\delta^{18}\text{O}$  of  $\sim 14\text{‰}$  at equilibrium [Buchwald and Casciotti, 2013]. As  $\text{NO}_2^-$  turnover in the coastal ODZ off Peru is relatively fast [Hu *et al.*, 2016], its  $\delta^{18}\text{O}$  likely would not have sufficient time to fully equilibrate with  $\text{H}_2\text{O}$  (see Figures S5c and S5d). However, even partial  $^{18}\text{O}$  equilibration with water could decrease the  $\delta^{18}\text{O}$  of  $\text{NO}_2^-$  and add a relatively low  $\delta^{18}\text{O}$  to the  $\text{N}_2\text{O}$  pool following  $\text{NO}_2^-$  reduction, affecting the relationship between  $\delta^{18}\text{O-N}_2\text{O}$  and  $\delta^{18}\text{O-NO}_3^-$  (Figures 7c and 7d) and potentially increasing the slope for SP versus  $\delta^{18}\text{O-N}_2\text{O}$  (see Figure 6a, transect A, where slope near 1 was observed). This was especially observed where  $\text{NO}_2^-$  significantly accumulated, and where  $\text{NO}_3^-$  was depleted and  $\delta^{18}\text{O-NO}_3^-$  high.

Our data also supported gross  $\text{N}_2\text{O}$  production even at the highest extent of N loss. Low SPs were observed where  $\text{NO}_3^-$  and  $\text{NO}_2^-$  were almost completely consumed and biogenic  $\text{N}_2$  was the highest in the ODZ at the shallowest stations 63 (transect A) and 9 (transect B) (Figure 6). At these stations, both  $\delta^{15}\text{N}^{\alpha}\text{-N}_2\text{O}$  and  $\delta^{15}\text{N}^{\beta}\text{-N}_2\text{O}$  were elevated and closer to the isotopic composition of the substrates ( $\text{NO}_3^-$  and  $\text{NO}_2^-$ ) when present.  $\Delta\text{N}_2\text{O}$  was also slightly above 0, i.e., equilibrium, at station 63, transect A ( $8 \text{ nmol L}^{-1}$ ) and station 9, transect B (up to  $11.5 \text{ nmol L}^{-1}$ ). As SP is not affected by the initial isotopic composition of the substrate nor fractionated during  $\text{N}_2\text{O}$  production [Sutka *et al.*, 2006], the observed low SPs, along with  $\text{N}_2\text{O}$  concentrations above equilibrium, suggest  $\text{N}_2\text{O}$  production in the ODZ at these shallow stations, in accordance with our model (Figure 8h). Organic matter, a substrate for denitrification (and hence  $\text{N}_2\text{O}$  production), decreases exponentially with depth below the euphotic zone [Martin *et al.*, 1987], potentially explaining the higher relative  $\text{N}_2\text{O}$  production (versus consumption) at these shallow stations.

For completeness, abiotic  $\text{N}_2\text{O}$  production by iron reduction of  $\text{NO}_2^-$  needs to be considered as a source of  $\text{N}_2\text{O}$  in the ODZ. Reduced iron as well as  $\text{NO}_2^-$  is present in the ODZ, making this reaction possible although there is currently no evidence for significant reaction rates. High SPs (30–36‰ [e.g., Toyoda *et al.*, 2005; Heil *et al.*, 2014]) are typically associated with abiotic  $\text{N}_2\text{O}$  production by various pathways involving the nitrification intermediates hydroxylamine or  $\text{NO}_2^-$  in combination with iron compounds or other transition metals. However, accounting for abiotic  $\text{N}_2\text{O}$  production in our box models suggested that this process did not significantly contribute to our observations, with the SP signature of  $\text{N}_2\text{O}$  production from metal reduction failing to predict the observed SP in most boxes for the computed mixing rates.

## 5. Summary and Concluding Remarks

We observed extreme  $\text{N}_2\text{O}$  concentrations of up to  $190 \text{ nmol L}^{-1}$  in surface waters off the Peru coast during December 2012 and January 2013, as previously reported by Arévalo-Martínez *et al.* [2015] and Kock *et al.* [2016].



We consistently observed low SPs in surface waters above the oxycline, mostly ranging from  $-3$  to  $14\text{‰}$ . Our model diagnosed biological fluxes suggested that nitrifier-denitrification or incomplete denitrifier-denitrification generally represented more than 50% of total  $\text{N}_2\text{O}$  production. While  $\text{N}_2\text{O}$  production by nitrifier-denitrification and denitrifier-denitrification have similar SP, making it impossible to distinguish between these two processes, several lines of evidence suggested that incomplete denitrifier-denitrification as waters are upwelled from the ODZ and re-oxygenated or nitrifier-denitrification fueled by  $\text{NO}_2^-$  from  $\text{NO}_3^-$  reduction in the ODZ are likely pathways for  $\text{N}_2\text{O}$  production in surface waters. Main indications were as follows: (1) the highest  $\text{N}_2\text{O}$  accumulations were observed in the PCW water mass, which is associated with upwelling; (2) there was no relationship between  $\Delta\text{N}_2\text{O}$  and AOU as expected for  $\text{N}_2\text{O}$  production by nitrification coupled to aerobic organic matter remineralization; and (3) we observed significant relationships between  $\delta^{15}\text{N}_{\text{bulk-N}_2\text{O}}$  and  $\delta^{15}\text{N}$  and  $\delta^{18}\text{O}$  of  $\text{NO}_3^-$ , a substrate for  $\text{N}_2\text{O}$  production during denitrification, above the oxycline. We estimated an efflux of up to  $0.6\text{ Tg N yr}^{-1}$  from nitrifier or incomplete denitrifier-denitrification, which is comparable to the estimate by Arévalo-Martínez *et al.* [2015].

We further used 3-D-reaction-advection-diffusion regional box models to investigate the rates and modes of  $\text{N}_2\text{O}$  production in surface waters and the rates of production and consumption in the ODZ. We estimated that a maximum of  $13\text{ Tg N yr}^{-1}$  could be removed in the coastal ODZ off Peru, which was about 23 times the maximum  $\text{N}_2\text{O}$  efflux. Our model diagnosed fluxes showed a decoupling between  $\text{N}_2\text{O}$  production and consumption, with generally higher relative  $\text{N}_2\text{O}$  consumption as biogenic  $\text{N}_2$  increased. A decrease or no change in  $\delta^{15}\text{N}^{\beta}\text{-N}_2\text{O}$  concomitant with increasing  $\delta^{15}\text{N}^{\alpha}$ ,  $\delta^{18}\text{O-N}_2\text{O}$ , and SP was generally observed in the ODZ. At the shallowest stations, at near substrate consumption, where the  $\delta^{15}\text{N}$  of  $\text{NO}_2^-$  and  $\text{NO}_3^-$  were also the highest, we observed high values for both  $\delta^{15}\text{N}^{\beta}\text{-N}_2\text{O}$  and  $\delta^{15}\text{N}^{\alpha}\text{-N}_2\text{O}$ , generally associated with low SPs.  $\text{N}_2\text{O}$  concentrations were also close or above equilibrium values at these stations. These observations likely indicated shifts from  $\text{N}_2\text{O}$  consumption to  $\text{N}_2\text{O}$  production in the ODZ, even at the highest extent of N loss.

Overall, our results show a strong spatial heterogeneity in the mechanisms controlling  $\text{N}_2\text{O}$  production and consumption in shallow waters off Peru, which should be better taken into account in global oceanic  $\text{N}_2\text{O}$  models.

## Acknowledgments

Data for this paper are available on the Data Management Portal for Kiel Marine Sciences hosted at GEOMAR (M91 and M92 cruises): <https://portal.geomar.de/>. This work was supported by the Deutsche Forschungsgemeinschaft project SFB-754 ([www.sfb754.de](http://www.sfb754.de)), SOPRANII (grant FKZ03F0611A; [www.sopran.pangaea.de](http://www.sopran.pangaea.de)), and a NSERC Postdoctoral Fellowship to A.B. R.T.L. was supported by DOE Office of Science grant DE-SC0016329. We would like to thank the captain and crew of R/V *Meteor* during the M91 and M92 cruises and Daniel Kieffer, Avi Bernales and Violeta Leon for their help during sampling. We thank the authorities of Peru for the permission to work in their territorial waters. The modeling part of the study has been conducted by using the Copernicus Marine Service Products.

## References

- Altabet, M. A. (2001), Nitrogen isotopic evidence for micronutrient control of fractional  $\text{NO}_3^-$  utilization in the equatorial Pacific, *Limnol. Oceanogr.*, *46*(2), 368–380.
- Altabet, M. A. (2006), Isotopic tracers of the marine nitrogen cycle: Present and past, in *Marine Organic Matter: Chemical and Biological Markers, Isotopes and DNA, The Handbook of Environmental Chemistry*, vol. 2N, edited by J. K. Volkman, chap. 8, pp. 251–293, Springer, Berlin.
- Arévalo-Martínez, D. L., A. Kock, C. R. Löscher, R. A. Schmitz, and H. W. Bange (2015), Massive nitrous oxide emissions from the tropical South Pacific Ocean, *Nat. Geosci.*, *8*(7), 530–533.
- Babbin, A. R., R. G. Keil, A. H. Devol, and B. B. Ward (2014), Organic matter stoichiometry, flux, and oxygen control nitrogen loss in the ocean, *Science*, *344*, 406–408.
- Babbin, A. R., D. Bianchi, A. Jayakumar, and B. B. Ward (2015), Rapid nitrous oxide cycling in the suboxic ocean, *Science*, *348*(6239), 1127–1129.
- Bange, H. W., S. Rapsomanikis, and M. O. Andreae (2001), Nitrous oxide cycling in the Arabian Sea, *J. Geophys. Res.*, *106*(C1), 1053–1065, doi:10.1029/1999JC000284.
- Barford, C. C., J. P. Montoya, M. A. Altabet, and R. Mitchell (1999), Steady-state nitrogen isotope effects of  $\text{N}_2$  and  $\text{N}_2\text{O}$  production in *Paracoccus denitrificans*, *Environ. Microbiol.*, *65*, 989–994.
- Barnier, B., L. Siefridt, and P. Marchesio (1995), Thermal forcing for a global ocean circulation model using a three-year climatology of ECMWF analyses, *J. Mar. Syst.*, *6*, 363–380.
- Bourbonnais, A., M. F. Lehmann, J. J. Waniek, and D. E. Schulz-Bull (2009), Nitrate isotope anomalies reflect  $\text{N}_2$  fixation in the Azores Front region (subtropical NE Atlantic), *J. Geophys. Res.*, *114*, C03003, doi:10.1029/2007JC004617.
- Bourbonnais, A., M. A. Altabet, C. N. Charoenpong, J. Larkum, H. Hu, H. W. Bange, and L. Stramma (2015), N-loss isotope effects in the Peru oxygen minimum zone studied using a mesoscale eddy as a natural tracer experiment, *Global Biogeochem. Cycles*, *29*, 793–811, doi:10.1002/2014GB005001.
- Brandes, J. A., A. H. Devol, T. Yoshinari, D. A. Jayakumar, and S. W. A. Naqvi (1998), Isotopic composition of nitrate in the central Arabian Sea and eastern tropical North Pacific: A tracer for mixing and nitrogen cycles, *Limnol. Oceanogr.*, *43*(7), 1680–1689.
- Brunner, B., et al. (2013), Nitrogen isotope effects induced by anammox bacteria, *Proc. Natl. Acad. Sci. U.S.A.*, *110*(47), 18,994–18,999.
- Bryan, B. A., G. Shearer, J. L. Skeeters, and D. H. Kohl (1983), Variable expression of the nitrogen isotope effect associated with denitrification of nitrite, *J. Biol. Chem.*, *258*, 8613–8617.
- Buchwald, C., and K. L. Casciotti (2013), Isotopic ratios of nitrite as tracers of the sources and age of oceanic nitrite, *Nat. Geosci.*, *6*(4), 308–313.
- Canfield, D. E., F. J. Stewart, B. Thamdrup, L. De Brabandere, T. Dalsgaard, E. F. Delong, N. P. Revsbech, and O. Ulloa (2010), A cryptic sulfur cycle in oxygen-minimum-zone waters off the Chilean coast, *Science*, *330*(6009), 1375–1378.

- Casciotti, K. L. (2009), Inverse kinetic isotope fractionation during bacterial nitrite oxidation, *Geochim. Cosmochim. Acta*, 73(7), 2061–2076.
- Casciotti, K. L., and M. R. McIlvin (2007), Isotopic analyses of nitrate and nitrite from reference mixtures and application to Eastern Tropical North Pacific waters, *Mar. Chem.*, 107(2), 184–201.
- Casciotti, K. L., D. M. Sigman, M. G. Hastings, J. K. Böhlke, and A. Hilkert (2002), Measurement of the oxygen isotopic composition of nitrate in seawater and freshwater using the denitrifier method, *Anal. Chem.*, 74(19), 4905–4912.
- Casciotti, K. L., J. K. Böhlke, M. R. McIlvin, S. J. Mroczkowski, and J. E. Hannon (2007), Oxygen isotopes in nitrite: Analysis, calibration, and equilibration, *Anal. Chem.*, 79(6), 2427–2436, doi:10.1021/ac061598h.
- Charoenpong, C. N., L. A. Bristow, and M. A. Altabet (2014), A continuous flow isotope ratio mass spectrometry method for high precision determination of dissolved gas ratios and isotopic composition, *Limnol. Oceanogr. Methods*, 12, 323–337.
- Ciais, P., et al. (2013), Carbon and other biogeochemical cycles, in *Climate Change 2013: The Physical Science Basis. Contribution of Working Group I to the Fifth Assessment Report of the Intergovernmental Panel on Climate Change*, edited by T. F. Stocker et al., Cambridge Univ. Press, Cambridge, U. K., and New York.
- Codispoti, L. A., J. A. Brandes, J. P. Christensen, A. H. Devol, S. W. A. Naqvi, H. W. Paerl, and T. Yoshinari (2001), The oceanic fixed nitrogen and nitrous oxide budgets: Moving targets as we enter the anthropocene?, *Sci. Mar.*, 65, 85–105.
- Cohen, Y., and L. I. Gordon (1978), Nitrous oxide in the oxygen minimum of the eastern tropical North Pacific: Evidence for its consumption during denitrification and possible mechanisms for its production, *Deep Sea Res.*, 25, 509–524.
- Cohen, Y., and L. I. Gordon (1979), Nitrous oxide production in the Ocean, *J. Geophys. Res.*, 84(C1), 347–353, doi:10.1029/JC084iC01p00347.
- Da Silva, A. M., C. C. Young, and S. Levitus (1994), Atlas of surface marine data 1994, vol. 1, Algorithms and procedures, technical report, Natl. Oceanogr. and Atmos. Admin., Silver, Spring, Md.
- Dalsgaard, T., F. J. Stewart, B. Thamdrup, L. De Brabandere, N. P. Revsbech, O. Ulloa, D. E. Canfield, and E. F. DeLong (2014), Oxygen at nanomolar levels reversibly suppresses process rates and gene expression in anammox and denitrification in the oxygen minimum zone off northern Chile, *MBio*, 5(6), e01966–14, doi:10.1128/mBio.01966-14.
- De Wilde, H. P. J., and W. Helder (1997), Nitrous oxide in the Somali Basin: The role of upwelling, *Deep Sea Res., Part II*, 44(6–7), 1319–1340.
- Echevin, V., F. Colas, A. Chaigneau, and P. Penven (2011), Sensitivity of the Northern Humboldt Current System nearshore modeled circulation to initial and boundary conditions, *J. Geophys. Res.*, 116, C07002, doi:10.1029/2010JC006684.
- Fariás, L., V. Besoain, and S. García-Loyola (2015), Presence of nitrous oxide hotspots in the coastal upwelling area off central Chile: An analysis of temporal variability based on ten years of a biogeochemical time series, *Environ. Res. Lett.*, 10(4), 1–13, doi:10.1088/1748-9326/10/4/044017.
- Forster, P., et al. (2007), Changes in atmospheric constituents and in radiative forcing, in *Climate Change 2007: The Physical Science Basis. Contribution of Working Group I to the Fourth Assessment Report of the Intergovernmental Panel on Climate Change*, edited by S. Solomon et al., Cambridge Univ. Press, Cambridge, U. K., and New York.
- Frame, C. H., and K. L. Casciotti (2010), Biogeochemical controls and isotopic signatures of nitrous oxide production by a marine ammonia-oxidizing bacterium, *Biogeosciences*, 7(9), 2695–2709.
- Frame, C. H., E. Deal, C. D. Nevison, and K. L. Casciotti (2014), N<sub>2</sub>O production in the eastern South Atlantic: Analysis of N<sub>2</sub>O stable isotopic and concentration data, *Global Biogeochem. Cycles*, 28, 1262–1278, doi:10.1002/2013GB004790.
- Freing, A., D. W. R. Wallace, and H. W. Bange (2012), Global oceanic production of nitrous oxide, *Philos. Trans. R. Soc. B: Biol. Sci.*, 367(1593), 1245–1255.
- Goreau, T. J., W. A. Kaplan, S. C. Wofsy, M. B. McElroy, F. W. Valois, and S. W. Watson (1980), Production of NO<sub>2</sub><sup>−</sup> and N<sub>2</sub>O by nitrifying bacteria at reduced concentrations of oxygen, *Appl. Environ. Microbiol.*, 40(3), 526–532.
- Granger, J., and D. M. Sigman (2009), Removal of nitrite with sulfamic acid for nitrate N and O isotope analysis with the denitrifier method, *Rapid Commun. Mass Spectrom.*, 23(23), 3753–3762.
- Granger, J., D. M. Sigman, J. A. Needoba, and P. J. Harrison (2004), Coupled nitrogen and oxygen isotope fractionation of nitrate during assimilation by cultures of marine phytoplankton, *Limnol. Oceanogr.*, 49(5), 1763–1773.
- Granger, J., D. M. Sigman, M. F. Lehmann, and P. D. Tortell (2008), Nitrogen and oxygen isotope fractionation during dissimilatory nitrate reduction by denitrifying bacteria, *Limnol. Oceanogr.*, 53(6), 2533–2545.
- Hamme, R. C., and S. R. Emerson (2002), Mechanisms controlling the global oceanic distribution of the inert gases argon, nitrogen and neon, *Geophys. Res. Lett.*, 29(23), 2120, doi:10.1029/2002GL015273.
- Heil, J., B. Wolf, N. Brüggemann, L. Emmenegger, B. Tuzson, H. Vereecken, and J. Mohn (2014), Site-specific <sup>15</sup>N isotopic signatures of abiotically produced N<sub>2</sub>O, *Geochim. Cosmochim. Acta*, 139(C), 72–82.
- Hu, H., A. Bourbonnais, J. Larkum, H. W. Bange, and M. A. Altabet (2016), Nitrogen cycling in shallow low-oxygen coastal waters off Peru from nitrite and nitrate nitrogen and oxygen isotopes, *Biogeosciences*, 13(5), 1453–1468, doi:10.5194/bg-13-1453-2016.
- Ji, Q., A. R. Babbitt, A. Jayakumar, S. Oleynik, and B. B. Ward (2015), Nitrous oxide production by nitrification and denitrification in the Eastern Tropical South Pacific oxygen minimum zone, *Geophys. Res. Lett.*, 42, 10,755–10,764, doi:10.1002/2015GL066853.
- Jinuntuya-Nortman, M., R. L. Sutka, P. H. Ostrom, H. Gandhi, and N. E. Ostrom (2008), Isotopologue fractionation during microbial reduction of N<sub>2</sub>O within soil mesocosms as a function of water-filled pore space, *Soil Biol. Biochem.*, 40, 2273–2280, doi:10.1016/j.soilbio.20.
- Kalvelage, T., M. M. Jensen, S. Contreras, N. P. Revsbech, P. Lam, M. Günter, J. LaRoche, G. Lavik, and M. M. M. Kuypers (2011), Oxygen sensitivity of anammox and coupled N-cycle processes in oxygen minimum zones, edited by J. A. Gilbert, *PLoS One*, 6(12), e29299, doi:10.1371/journal.pone.0029299.t003.
- Kalvelage, T., G. Lavik, P. Lam, S. Contreras, L. Arteaga, C. R. Löscher, A. Oschlies, A. Paulmier, L. Stramma, and M. M. M. Kuypers (2013), Nitrogen cycling driven by organic matter export in the South Pacific oxygen minimum zone, *Nat. Geosci.*, 6(3), 228–234.
- Kock, A., D. L. Arévalo-Martínez, C. R. Löscher, and H. W. Bange (2016), Differences between coastal and open ocean distributions of N<sub>2</sub>O in the oxygen minimum zone off Peru, *Biogeosciences*, 13, 827–840.
- Kool, D. M., J. W. Van Groenigen, and N. Wragge (2011), Source determination of nitrous oxide based on nitrogen and oxygen isotope tracing: Dealing with oxygen exchange, in *Methods in Enzymology*, vol. 496, edited by M. G. Klotz and L. Y. Stein, pp. 139–160, Academic Press, Burlington.
- Law, C. S., and N. J. P. Owens (1990), Significant flux of atmospheric nitrous oxide from the northwest Indian Ocean, *Nature*, 346, 826–828.
- Lewicka-Szczepak, D., R. Well, R. Bol, A. S. Gregory, G. P. Matthews, T. Misselbrook, W. R. Whalley, and L. M. Cardenas (2015), Isotope fractionation factors controlling isotopocule signatures of soil-emitted N<sub>2</sub>O produced by denitrification processes of various rates, *Rapid Commun. Mass Spectrom.*, 29, 269–282.
- Löscher, C. R., A. Kock, M. Könneke, J. LaRoche, H. W. Bange, and R. A. Schmitz (2012), Production of oceanic nitrous oxide by ammonia-oxidizing archaea, *Biogeosciences*, 9(7), 2419–2429.



- Mandernack, K. W., T. Rahn, C. Kinney, and M. Wahlen (2000), The biogeochemical controls of the  $\delta^{15}\text{N}$  and  $\delta^{18}\text{O}$  of  $\text{N}_2\text{O}$  produced in landfill cover soils, *J. Geophys. Res.*, 105(D14), 17,709–720, doi:10.1029/2000JD900055.
- Martin, J. H., G. A. Knauer, D. M. Karl, and W. W. Broenkow (1987), VERTEX: Carbon cycling in the northeast Pacific, *Deep Sea Res. Part A*, 34, 267–285.
- McIlvin, M. R., and K. L. Casciotti (2010), Fully automated system for stable isotopic analyses of dissolved nitrous oxide at natural abundance levels, *Limnol. Oceanogr. Methods*, 8, 54–66.
- McIlvin, M. R., and M. A. Altabet (2005), Chemical conversion of nitrate and nitrite to nitrous oxide for nitrogen and oxygen isotopic analysis in freshwater and seawater, *Anal. Chem.*, 77(17), 5589–5595.
- Menyailo, O. V., and B. A. Hungate (2006), Stable isotope discrimination during soil denitrification: Production and consumption of nitrous oxide, *Global Biogeochem. Cycles*, 20, GB3025, doi:10.1029/2005GB002527.
- Mohn, J., et al. (2014), Inter-laboratory assessment of nitrous oxide isotopomer analysis by isotope ratio mass spectrometry and laser spectroscopy: Current status and perspectives, *Rapid Commun. Mass Spectrom.*, 28(18), 1995–2007.
- Montes, I., W. Schneider, F. Colas, B. Blanke, and V. Echevin (2011), Subsurface connections in the eastern tropical Pacific during La Niña 1999–2001 and El Niño 2002–2003, *J. Geophys. Res.*, 116, C12022, doi:10.1029/2011JC007624.
- Naqvi, S. W. A., D. A. Jayakumar, P. V. Narvekar, H. Naik, V. V. S. S. Sarma, W. D'Souza, S. Joseph, and M. D. George (2000), Increased marine production of  $\text{N}_2\text{O}$  due to intensifying anoxia on the Indian continental shelf, *Nature*, 408, 346–349.
- Naqvi, S. W. A., H. W. Bange, L. Farias, P. M. S. Monteiro, M. I. Scranton, and J. Zhang (2010), Marine hypoxia/anoxia as a source of  $\text{CH}_4$  and  $\text{N}_2\text{O}$ , *Biogeosciences*, 7(7), 2159–2190.
- Nevison, C. D., and E. Holland (1997), A reexamination of the impact of anthropogenically fixed nitrogen on atmospheric  $\text{N}_2\text{O}$  and the stratospheric  $\text{O}_2$  layer, *J. Geophys. Res.*, 102(D21), 25,519–25,536, doi:10.1029/97JD02391.
- Nevison, C. D., R. F. Weiss, and D. J. Erickson III (1995), Global oceanic emissions of nitrous oxide, *J. Geophys. Res.*, 100(C8), 15,809–15,820, doi:10.1029/95JC00684.
- Nevison, C. D., T. J. Lueker, and R. F. Weiss (2004), Quantifying the nitrous oxide source from coastal upwelling, *Global Biogeochem. Cycles*, 18, GB1018, doi:10.1029/2003GB002110.
- Nevison, C., J. H. Butler, and J. W. Elkins (2003), Global distribution of  $\text{N}_2\text{O}$  and the  $\Delta\text{N}_2\text{O}$ -AOU yield in the subsurface ocean, *Global Biogeochem. Cycles*, 17(4), 1119, doi:10.1029/2003GB002068.
- Ostrom, N. E., A. Pitt, R. Sutka, P. H. Ostrom, A. S. Grandy, K. M. Huizinga, and G. P. Robertson (2007), Isotopologue effects during  $\text{N}_2\text{O}$  reduction in soils and in pure cultures of denitrifiers, *J. Geophys. Res.*, 112, G02005, doi:10.1029/2006JG000287.
- Ostrom, N., and P. Ostrom (2011), The isotopomers of nitrous oxide: analytical considerations and application to resolution of microbial production pathways, in *Handbook of Environmental Isotope Geochemistry – Advances in Isotope Geochemistry*, Part 1, edited by M. Baskaran, pp. 453–476, Springer, Berlin.
- Penven, P., V. Echevin, J. Pasapera, F. Colas, and J. Tam (2005), Average circulation, seasonal cycle, and mesoscale dynamics of the Peru Current System: A modeling approach, *J. Geophys. Res.*, 110, C10021, doi:10.1029/2005JC002945.
- Pietri, A., V. Echevin, P. Testor, A. Chaigneau, L. Mortier, C. Grados, and A. Albert (2014), Impact of a coastal-trapped wave on the near-coastal circulation of the Peru upwelling system from glider data, *J. Geophys. Res. Oceans*, 119, 2109–2120, doi:10.1002/2013JC009270.
- Ravishankara, A. R., J. S. Daniel, and R. W. Portmann (2009), Nitrous oxide ( $\text{N}_2\text{O}$ ): The dominant ozone-depleting substance emitted in the 21st century, *Science*, 326(5949), 123–125.
- Ryabenko, E., A. Kock, H. W. Bange, M. A. Altabet, and D. W. R. Wallace (2012), Contrasting biogeochemistry of nitrogen in the Atlantic and Pacific oxygen minimum zones, *Biogeosciences*, 9(1), 203–215.
- Santoro, A. E., K. L. Casciotti, and C. A. Francis (2010), Activity, abundance and diversity of nitrifying archaea and bacteria in the central California Current, *Environ. Microbiol.*, 12(7), 1989–2006.
- Santoro, A. E., C. Buchwald, M. R. McIlvin, and K. L. Casciotti (2011), Isotopic signature of  $\text{N}_2\text{O}$  produced by marine ammonia-oxidizing Archaea, *Science*, 333, 1282–1285.
- Schmidt, H.-L., R. A. Werner, N. Yoshida, and R. Well (2004), Is the isotopic composition of nitrous oxide an indicator for its origin from nitrification or denitrification? A theoretical approach from referred data and microbiological and enzyme kinetic aspects, *Rapid Commun. Mass Spectrom.*, 18(18), 2036–2040.
- Shchepetkin, A. F., and J. C. McWilliams (2005), The regional oceanic modeling system (ROMS): A split-explicit, free-surface, topography-following-coordinate oceanic model, *Ocean Model.*, 9, 347–404.
- Sigman, D. M., K. L. Casciotti, M. Andreani, C. Barford, M. Galanter, and J. K. Böhlke (2001), A bacterial method for the nitrogen isotopic analysis of nitrate in seawater and freshwater, *Anal. Chem.*, 73(17), 4145–4153.
- Sigman, D. M., J. Granger, P. J. DiFiore, M. M. Lehmann, R. Ho, G. Cane, and A. van Geen (2005), Coupled nitrogen and oxygen isotope measurements of nitrate along the eastern North Pacific margin, *Global Biogeochem. Cycles*, 19, GB4022, doi:10.1029/2005GB002458.
- Snider, D. M., J. J. Venkiteswaran, S. L. Schiff, and J. Spoelstra (2012), Deciphering the oxygen isotope composition of nitrous oxide produced by nitrification, *Glob. Chang. Biol.*, 18, 356–370.
- Stramma, L., H. W. Bange, R. Czeschel, A. Lorenzo, and M. Frank (2013), On the role of mesoscale eddies for the biological productivity and biogeochemistry in the eastern tropical Pacific Ocean off Peru, *Biogeosciences*, 10, 7293–7306.
- Strub, P. T., J. M. Mesías, V. Montecino, J. Rutilliant, and S. Salinas (1998), Coastal ocean circulation off western south America, in *The Sea*, vol. 11, edited by A. R. Robinson and K. H. Brink, pp. 273–313, John Wiley, New York.
- Sutka, R. L., N. E. Ostrom, P. H. Ostrom, H. Gandhi, and J. A. Breznak (2003), Nitrogen isotopomer site preference of  $\text{N}_2\text{O}$  produced by *Nitrosomonas europaea* and *Methylococcus capsulatus* Bath, *Rapid Commun. Mass Spectrom.*, 17, 738–745.
- Sutka, R. L., N. E. Ostrom, P. H. Ostrom, H. Gandhi, and J. A. Breznak (2004), Erratum: Nitrogen isotopomer site preference of  $\text{N}_2\text{O}$  produced by *Nitrosomonas europaea* and *Methylococcus capsulatus* Bath, *Rapid Commun. Mass Spectrom.*, 18, 1411–1412.
- Sutka, R. L., N. E. Ostrom, P. H. Ostrom, J. A. Breznak, H. Gandhi, A. J. Pitt, and F. Li (2006), Distinguishing nitrous oxide production from nitrification and denitrification on the basis of isotopomer abundances, *Appl. Environ. Microbiol.*, 72(1), 638–644.
- Toyoda, S., N. Yoshida, T. Miwa, Y. Matsui, H. Yamagishi, U. Tsunogai, Y. Nojiri, and N. Tsurushima (2002), Production mechanism and global budget of  $\text{N}_2\text{O}$  inferred from its isotopomers in the western North Pacific, *Geophys. Res. Lett.*, 29(3), 1037, doi:10.1029/2001GL014311.
- Toyoda, S., H. Mutoke, H. Yamagishi, N. Yoshida, and Y. Tanji (2005), Fractionation of  $\text{N}_2\text{O}$  isotopomers during production by denitrifier, *Soil Biol. Biochem.*, 37(8), 1535–1545.
- Toyoda, S., N. Kuroki, N. Yoshida, K. Ishijima, Y. Tohjima, and T. Machida (2013), Decadal time series of tropospheric abundance of  $\text{N}_2\text{O}$  isotopomers and isotopologues in the Northern Hemisphere obtained by the long-term observation at Hateruma Island, Japan, *J. Geophys. Res. Atmos.*, 118, 3369–3381, doi:10.1002/jgrd.50221.
- Upstill-Goddard, R. C., J. Barnes, and N. J. P. Owens (1999), Nitrous oxide and methane during the 1994 SW monsoon in the Arabian Sea/northwestern Indian Ocean, *J. Geophys. Res.*, 104(C12), 30,067–30,084, doi:10.1029/1999JC900232.

- Voss, M., J. W. Dippner, and J. Montoya (2001), Nitrogen isotope patterns in the oxygen-deficient waters of the Eastern Tropical North Pacific Ocean, *Deep Sea Res., Part I*, 48, 1905–1921.
- Weiss, R. F., and B. A. Price (1980), Nitrous oxide solubility in water and seawater, *Mar. Chem.*, 8, 347–359.
- Westley, M. B., H. Yamagishi, B. N. Popp, and N. Yoshida (2006), Nitrous oxide cycling in the Black Sea inferred from stable isotope and isotopomer distributions, *Deep Sea Res., Part II*, 53(17–19), 1802–1816.
- Westley, M. B., B. N. Popp, and T. M. Rust (2007), The calibration of the intramolecular nitrogen isotope distribution in nitrous oxide measured by isotope ratio mass spectrometry, *Rapid Commun. Mass Spectrom.*, 21(3), 391–405.
- Wrage, N., J. W. Van Groenigen, O. Oenema, and E. M. Baggs (2005), A novel dual-isotope labelling method for distinguishing between soil sources of N<sub>2</sub>O, *Rapid Commun. Mass Spectrom.*, 19(22), 3298–3306.
- Yamagishi, H., N. Yoshida, S. Toyoda, B. N. Popp, M. B. Westley, and S. Watanabe (2005), Contributions of denitrification and mixing on the distribution of nitrous oxide in the North Pacific, *Geophys. Res. Lett.*, 32, L04603, doi:10.1029/2004GL021458.
- Yamagishi, H., M. B. Westley, B. N. Popp, S. Toyoda, N. Yoshida, S. Watanabe, K. Koba, and Y. Yamanaka (2007), Role of nitrification and denitrification on the nitrous oxide cycle in the eastern tropical North Pacific and Gulf of California, *J. Geophys. Res.*, 112, G02015, doi:10.1029/2006JG000227.
- Yoshida, N., and S. Toyoda (2000), Constraining the atmospheric N<sub>2</sub>O budget from intramolecular site preference in N<sub>2</sub>O isotopomers, *Nature*, 405, 330–334.
- Yoshida, N., H. Morimoto, M. Hirano, I. Koike, S. Matsuo, E. Wada, T. Saino, and A. Hattori (1989), Nitrification rates and <sup>15</sup>N abundances of N<sub>2</sub>O and NO<sub>3</sub><sup>−</sup> in the western North Pacific, *Nature*, 342, 895–897.
- Yoshinari, T. (1976), Nitrous oxide in the Sea, *Mar. Chem.*, 4, 189–202.
- Zamora, L. M., A. Oschlies, H. W. Bange, K. B. Huebert, J. D. Craig, A. Kock, and C. R. Löscher (2012), Nitrous oxide dynamics in low oxygen regions of the Pacific: Insights from the MEMENTO database, *Biogeosciences*, 9(12), 5007–5022.